Unraveling phenological and stomatal responses to flash drought and implications for water and carbon budgets

Nicholas K. Corak[1,2], Jason A. Otkin[3], Trent W. Ford[4], and Lauren E. L. Lowman[1,2]

[1]Department of Physics, Wake Forest University, Winston-Salem, NC, USA
[2]Department of Engineering, Wake Forest University, Winston-Salem, NC, USA
[3]Cooperative Institute for Meteorological Satellite Studies, Space Science and Engineering Center, University of Wisconsin-Madison, Madison, WI, USA
[4]Illinois State Water Survey, Prairie Research Institute, University of Illinois at Urbana-Champaign, Urbana-Champaign, IL, USA

Correspondence: Lauren E. L. Lowman (lowmanle@wfu.edu)

Abstract. In recent years, extreme droughts in the United States have increased in frequency and severity underlining a need to improve our understanding of vegetation resilience and adaptation. Flash droughts are extreme events marked by the rapid dry down of soils due to lack of precipitation, high temperatures, and dry air. These events are also associated with reduced preparation, response, and management time windows before and during drought which exacerbate their detrimental impacts on people and food systems. Improvements in actionable information for flash drought management are informed by atmospheric and land surface processes, including responses and feedbacks from vegetation. Phenologic state, or growth stage, is an important metric for modeling how vegetation modulates land-atmosphere interactions. Reduced stomatal conductance during drought leads to cascading effects on carbon and water fluxes. We investigate how uncertainty in vegetation phenology and stomatal regulation propagates through vegetation responses during drought and non-drought periods by coupling a land-surface hydrology model to a predictive phenology model. We assess the role of vegetation in the partitioning of carbon, water, and energy fluxes during flash drought and compare against drought and non-drought periods. We selected study sites in Kansas, USA that were impacted by the flash drought of 2012, and where AmeriFlux eddy covariance towers provide ground observations to compare against model estimates. Results show the compounding effects of reduced precipitation and high vapor pressure deficit (VPD) on vegetation distinguish flash drought from other drought and non-drought periods. High VPD during flash drought shuts down modeled stomatal conductance resulting in rates of evapotranspiration (ET), gross primary productivity (GPP), and water-use efficiency (WUE) falling below average drought conditions. Model estimates of GPP and ET during flash drought reduce to rates similar to what is observed during the winter indicating that plant function during drought periods is similar to those of dormant months. These results have implications for improving predictions of drought impacts on vegetation.

1 Introduction

The frequency and severity of extreme droughts are predicted to increase within the next century (Dai, 2013). Flash droughts are a particular type of extreme drought characterized by their rapid intensification (Svoboda et al., 2002; Ford and Labosier, 2017; Otkin et al., 2018, 2022). The flash drought of 2012 that impacted the Central United States amplified the need to understand and predict flash droughts because of its estimated \$30 billion of impacts to agriculture (Otkin et al., 2018). Work over the last decade has improved methods for identifying flash droughts based on rates of intensification of dry soils and concurrent elevated temperatures and atmospheric aridity (see Christian et al. (2024) and Lisonbee et al. (2021) for a summary of flash drought definitions and indicators). Many studies have examined the drivers (e.g., lack of precipitation, greater atmospheric demand for water, above average temperatures) and impacts (e.g., soil moisture deficits and damages to agriculture) of flash drought (e.g., Lowman et al., 2023; Christian et al., 2023, 2022; Jin et al., 2019; Otkin et al., 2018), while others have examined vegetation-atmosphere interactions (Hosseini et al., 2022; Chen et al., 2021; Zhang and Yuan, 2020; Gerken et al., 2018; Otkin et al., 2016), and stomatal functioning (Novick et al., 2016; Roman et al., 2015). This study addresses the need to bring together the physical mechanisms driving flash drought and the resulting vegetation responses that inform land-atmosphere interactions.

Further assessment of vegetation-atmosphere feedback mechanisms may help improve identification of flash drought onset (Qing et al., 2022). Gross primary productivity (GPP), or carbon assimilation by plants during photosynthesis, is one such vegetation-atmospheric interaction impacted by drought (Zeng et al., 2023). Large reductions in GPP due to soil moisture and temperature anomalies can be used to mark the beginning and duration of flash drought events (Poonia et al., 2022; Zhang and Yuan, 2020), as seen in the 2012 flash drought (Jin et al., 2019). Flash droughts can intensify through land-atmosphere feedbacks (Basara et al., 2019); for example, vegetation expediting water stress by pulling water from deeper soil layers and further drying soils (Qing et al., 2022). Otkin et al. (2016) studied the evolution of soil moisture and vegetation conditions during the 2012 event, finding that changes in soil moisture and evaporative stress indicators preceded rapid drought intensification in the US Drought Monitor (USDM, Svoboda et al. (2002)). Chen et al. (2019) found declines in evapotranspiration (ET), another interaction between the vegetation and the atmosphere, to be a major sign of flash drought intensification.

Interactions between vegetation and the atmosphere are altered during flash drought events, thus it is necessary to consider vegetation state when studying the effects of flash drought (Chen et al., 2021). Additionally, capturing differences across plant types is essential for modeling vegetation response to drought. Failure to account for differential responses across plant functional types (PFTs) could result in underestimating the plant's ability to maintain its function under water stress (Zhou et al., 2013). Roman et al. (2015) showed that tree species in a forested region behaved differently during drought, with some species exhibiting isohydric tendencies, whereas others were more anisohydric. Isohydric plants are more conservative with their water-use strategies when under stress and tend to regulate their stomatal conductance making them less susceptible to hydraulic failure (Konings and Gentine, 2017). These tendencies dictate how much photosynthesis occurs and thus how much carbon is exchanged (Roman et al., 2015). However, Garcia-Forner et al. (2017) cautions against making links between carbon assimilation and water potential regulation by showing similar rates of carbon assimilation under controlled drought simulations between two species of Mediterranean trees with opposing drought responses (one isohydric and one anisohydric). For

some species, stomatal regulation exists on a spectrum and can shift between isohydric and anisohydric in response to atmo-
spheric and water conditions (Wu et al., 2021; Guo et al., 2020), leading to variation and uncertainties in water-use strategies
(Kannenberg et al., 2022). Ecosystem scale modeling may be able to incorporate the plant level spatial and temporal variability
in water-use strategies (Giardina et al., 2023; Konings and Gentine, 2017), taking into account concurrent meteorological and
environmental conditions that influence plant water-use tendencies beyond the specie's physiological characteristics (Hochberg
et al., 2018).

Vegetation type and growth stage can play an important role in determining whether and how an area experiences changes
in carbon uptake during flash drought. There is evidence connecting vegetation changes in response to flash drought to lower
plant production (Zhang et al., 2020; Jin et al., 2019; He et al., 2018; Otkin et al., 2016; Hunt et al., 2014). Jin et al. (2019)
and He et al. (2018) found that croplands, grasslands, and shrublands experienced the majority of loss to carbon uptake rates
during the droughts of 2011 and 2012 across the central US and similar rates of ET were found in croplands in the US northern
plain flash drought of 2017 (He et al., 2019; Kimball et al., 2019). Chen et al. (2021) showed increases in LAI led to increased
ET and that in a low moisture regime the amount of latent heat released due to ET was sensitive to changes in LAI. Hunt et al.
(2014) showed that maize experienced decreases in stomatal conductance, which led to declines in GPP and ET, during a flash
drought. Roman et al. (2015) show that species specific stomatal control can lead to different drought responses implying some
plants that exhibit more drought tolerant behavior might be accessing deeper stores of water (Giardina et al., 2023).

Previous studies have used remotely sensed or ground measurements as indicators to study vegetation responses to flash
drought (e.g., Christian et al., 2022; Zhang et al., 2020; Basara et al., 2019). In contrast, Chen et al. (2021) used an earth system
model to gauge plant behavior during flash drought while Hosseini et al. (2022) used models with different phenological forcing
to investigate impacts on the water and carbon cycles during drought. Remotely sensed and eddy covariance data provide
snapshots of the state of the system at point-scale or gridded spatial resolutions, and fixed temporal resolutions, while models
can scale in space and time. Inherently simplified due to the complexity of systems, numerical models incorporate physical and
biological processes and statistical techniques to make predictions based on current states and their uncertainties (Dietze, 2017).
Data assimilation procedures and Bayesian inference allow modelers to incorporate observations while identifying sources of
uncertainty in both processes and scale (Dietze, 2017; Dietze et al., 2013).

Accurately capturing plant phenology has implications for estimating photosynthetic activity (Lowman and Barros, 2018, 2016;
Stöckli et al., 2008; Jolly et al., 2005), which will influence the water, carbon, and energy fluxes coupled between the land and
atmosphere. We use two versions of the Duke Coupled Land-Surface Hydrology Model (DCHM) that incorporate routines
for photosynthesis (Garcia-Quijano and Barros, 2005; Gebremichael and Barros, 2006), and predictive phenology, or plant
life stage (Lowman and Barros, 2018, 2016), to more closely investigate if and how vegetation water-use strategies accelerate
or decelerate dry down before and during flash drought. Data assimilation techniques allow us to capture model uncertainty
around processes controlling vegetation activity, and in particular, assimilating vegetation phenology can improve the detec-
tion of drought (Mocko et al., 2021). We investigate whether plants exhibit anisohydric tendencies thereby exacerbating the
dry down, or whether they regulate their water intake to preserve soil moisture and mitigate the effects of flash drought. In
turn, we explore if plant behavior can be altered during periods of water stress by predicting phenology model parameters from

hydrologic model outputs in dry and wet periods. We hypothesize that simulated transpiration and carbon uptake rates will
taper during flash drought due to limited soil water availability and increased atmospheric demand and that the phenological
changes are directly related to changes in transpiration rates and GPP (Figure 1). Our specific hypotheses are:

H1 During flash drought, there is an increase in days between precipitation events leading to larger reductions in total precipitation and infiltration as compared to non-flash drought events.

H2 Lower total infiltration and higher atmospheric demand for water observed during flash drought reduces soil water available for root water uptake. This decreases stomatal conductance, subsequently leading to reduced rates of transpiration, carbon uptake, and water-use efficiency as compared to non-flash drought within a subseasonal time frame.

H3 In response to decreased water availability during flash drought, vegetation phenological states will be diminished as compared to non-flash drought years exacerbating the reduction of transpiration and carbon uptake.

Here we use phenological responses of fraction of photosynthetically active radiation (FPAR) and leaf area index (LAI) to examine how flash droughts affect vegetation state and ultimately impact the surface fluxes governing the movement of water and carbon between the land and atmosphere. We use the well-studied flash drought of 2012 to compare vegetation growth state and water-use strategies during flash drought and non-drought periods to better understand how plants modulate water and interact with the atmosphere when under stress. Specifically, the model is used to explore how phenological state and stomatal regulation are altered by flash drought and subsequently affect vegetation productivity. We compare our model results with eddy covariance and remotely sensed values of vegetation state and atmospheric interactions. Discrepancies between observations and models with predictive versus forced phenology illuminate physical processes dictating plant water-use strategies (e.g., suppressing transpiration by closing stomata and limiting carbon intake). This study extends previous research on the water and carbon movement between plants and the atmosphere during flash drought by simulating the propagation of uncertainty after implementing a predictive phenology routine to understand how variability in the representation of vegetation state within a modeling framework impacts land-atmosphere exchanges during extreme drought events.

2 Methods and Data

2.1 Overview of Modeling Approach

Remotely sensed or ground observations of land and atmospheric responses to flash drought are useful in identifying changes in plant phenology, soil moisture, and evaporation rates, among others, but observations alone are unable to fully explain the mechanisms driving ecological responses and water-use strategies. Physically-based models can help fill the gaps in understanding what drives these changes by identifying key processes in the land-atmosphere interactions. For example, decreases in ground-based or satellite-derived GPP do not illuminate what processes caused the change, whereas a process based model might be able to signal that changes in root water uptake lead to decreased transpiration rates, which ultimately lead to decreased photosynthesis and carbon assimilation.
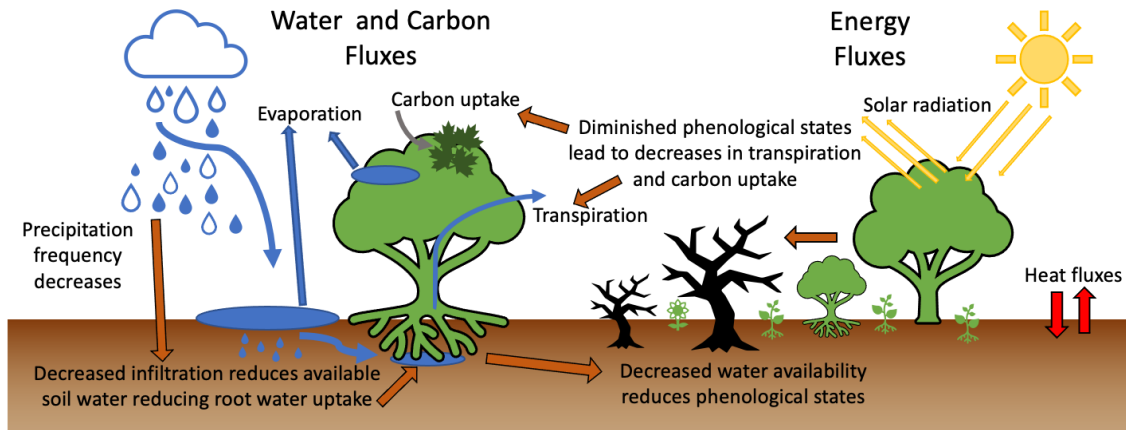
Figure 1. Schematic of water, carbon, and energy fluxes with hypotheses about ecohydrological response to flash drought indicated with orange arrows. Decreased frequency of precipitation events leads to decreased infiltration and less water available for plant use during flash drought as compared to non-flash drought periods. During flash drought, the cascading effects of decreased water availability, exacerbated by the reduced phenological states and stomatal conductance, include rapid reductions in transpiration and atmospheric carbon uptake to levels below other drought periods.

Within physical models, changes in land-surface variables (e.g., soil moisture, root uptake, evaporation rates, etc.) are dependent upon meteorological conditions, either forced or dynamic (Sellers et al., 1997). Water-use strategies are dictated by vegetation phenological states (Hu et al., 2008) and stomatal regulation (Novick et al., 2016), and they strongly influence GPP and ET (Beer et al., 2009). Therefore, physical, process-based models are able to adapt to changing meteorological conditions and capture mechanistic changes in vegetation-atmosphere interactions. Our goal is to identify vegetation responses that occur as a result of flash drought and associate those changes with the physical processes represented in a land-surface hydrology model.

To identify physical mechanisms driving plant responses to flash drought intensification, we use two configurations of the physically based Duke Coupled surface-subsurface Hydrology Model (DCHM) with dynamic Vegetation (DCHM-V) and Predictive Vegetation (DCHM-PV). The DCHM-V provides baseline estimates soil moisture (SM), root uptake (RU), ET, and GPP using forced phenology from the from Moderate Resolution Imaging Spectroradiometer (MODIS) FPAR and LAI products. Instead of using forced phenology, the DCHM-PV uses a prognostic vegetation (i.e. phenological) model to predict the vegetation states of FPAR and LAI using parameters that correspond to seasonality (e.g., temperature and photoperiod), water availability (e.g., soil and vapor pressure deficit), and local vegetation characteristics (Lowman and Barros, 2018; Kim et al., 2015; Caldararu et al., 2014; Stöckli et al., 2008; Moradkhani et al., 2005). An ensemble Kalman filter (EnKF) data assimilation procedure following Lowman and Barros (2018) is used to estimate ensembles of parameters for use in the predictive phenology model. Monte Carlo simulations of the DCHM-PV with the ensembles of predictive phenology parameters from the data assimilation step are used to explore the propagation of error and uncertainty. We validate model simulations against

ground observations, remotely sensing data, and other modeled products. A summary of the data sets used to force or validate both configurations of the DCHM is provided in Table 1.

Table 1. Summary of data products and uses

Dataset	Variable(s)	Spatial Resolution	Temporal Resolution	Use	Reference
Stage-IV	precipitation	4 km	1 h	forcing	Baldwin and Mitchell (1998); Du (2011)
NLDAS-2 Forcing File A	wind speed, air pressure, temperature, specific humidity, incoming shortwave and long wave radiation	0.125°	1 h	forcing/data assimilation	Mitchell et al. (2004)
NLDAS-2 Mosaic	vegetation fraction/ albedo	0.125°	1 h	forcing/data assimilation	Xia et al. (2012)
MODIS MOD15A2H	LAI/FPAR	500 m	8 day	forcing/data assimilation	Myneni et al. (2015)
MODIS MOD12Q1	land cover	500 m	yearly	forcing	Friedl and Sulla-Menashe (2015)
STATSGO	soil texture/porosity	30 arcsec	fixed	forcing	Miller and White (1998)
AmeriFlux	GPP, latent heat, SM	point	30 min.	validation	Baldocchi et al. (2001)
MODIS MOD17A2H	GPP	500 m	8 day	validation	Running et al. (2015)
NLDAS-2	SM	0.125°	1 h	validation	Xia et al. (2012)
SMERGE	SM	0.125°	1 h	validation	Tobin et al. (2019)

2.2 Forcing Data Sets for the DCHM

2.2.1 Meteorological

The 1-D DCHM-V and -PV spatial and temporal resolution is set to the same scale as the highest quality precipitation forcing data available. For this study, the model uses the native resolution of the Stage-IV precipitation forcing from the National Oceanic and Atmospheric Administration (NOAA) National Centers for Environmental Prediction (NCEP) (Baldwin and

145   Mitchell, 1998; Du, 2011). The Stage-IV dataset has 4 km spatial resolution and 1 h temporal resolution and with a record beginning in 2002. All forcing data sets were interpolated to the Stage-IV resolution for the entire continental US (CONUS) before study site specific data were extracted. Atmospheric forcing data (downward short and long wave radiation, air temperature, specific humidity, surface pressure, wind velocity) used in the DCHM are from the North America Land Data Assimilation System Phase 2 (NLDAS-2) Forcing File A (Mitchell et al., 2004). NLDAS-2 is a combination of observational and reanalysis

150   data sets intended for use in land surface models like the DCHM. The data are available at 0.125 degree spatial resolution and 1 h temporal resolution. They are spatially interpolated to the 4 km Stage-IV grid. No temporal interpolation was necessary.

2.2.2   Land Cover

The land surface albedo and fraction of vegetation cover used in the DCHM-V and -PV come from the NLDAS-2 Mosaic Land Surface Model L4 dataset at 0.125 degree spatial resolution and 1 h temporal resolution (Xia et al., 2012; Mitchell et al., 2004).

155   NASA's MODIS Land Cover (MCD12Q1) remotely sensed satellite land cover classification product is used to determine land cover type within the DCHM. In particular, we use the University of Maryland classification scheme (Sulla-Menashe and Friedl, 2018). Within the model, land cover type is updated yearly. The native spatial resolution of this data set is 500 m and it is interpolated to the 4 km resolution using a nearest neighbor approach.

2.2.3   Soil Texture and Porosity

160   Soil texture and porosity data was acquired from Soil Information for Environmental Modeling and Ecosystem Management CONUS-Soil (Miller and White, 1998). The CONUS-Soil spatial resolution is 1 km with 11 layers. We upscaled the raw soil texture and porosity data to the 4-km Stage-IV grid using two different methods. By averaging over the top 100 cm, we avoid averaging layers interpolated as bedrock, and thus near zero porosity. We approximate soil porosity by averaging the top eight layers (100 cm) and we represent texture using the texture mode across each grid cell and layer.

165 ### 2.2.4   Vegetation

MODIS LAI and FPAR data were obtained for all of CONUS at the native 500-m spatial and 8-day temporal resolution. Before linearly interpolating the data to the Stage-IV grid and timestep, the data for each pixel were smoothed using a Savitsky-Golay filter (Savitzky and Golay, 1964), following the algorithm presented in Chen et al. (2004), in order to preserve seasonality and reduce noise in the data from cloud contamination and other atmospheric disturbances that may alter surface reflectance obser-

170   vations (Cihlar et al., 1997; Tanré et al., 1997). We use m=6 scaling window and d=4 degree for the interpolating polynomial (Chen et al., 2004; Lowman and Barros, 2016).

2.3   Data Sets Used for Model Comparison

We assess vegetation responses to the Kansas flash drought of 2012 by comparing model results of land surface, sub-surface and atmospheric carbon and water fluxes (e.g., SM, GPP, ET) to multiple ground and remotely sensed observations. Modeled SM

175 fluxes from the DCHM-V and -PV are compared to SoilMERGE (SMERGE), NLDAS-2 NOAH model output, and AmeriFlux eddy covariance. SMERGE is a 0.125 degree root-zone (0-40 cm) SM product obtained from 'merging' NLDAS-2 outputs with European Space Agency Climate Change Initiative surface satellite data that can predict vegetation health anomalies (Tobin et al., 2019). Because SMERGE only provides root-zone SM, we only compare it to the DCHM middle layer SM output. We also validate SM estimates against NLDAS-2 estimates Noah land-surface model (LSM) for all three soil layers used in DCHM

180 (Xia et al., 2012)). When AmeriFlux SM data is available, we compare with modeled soil moisture from the top layer since most AmeriFlux SM sensors are in the top few centimeters of soil. The DCHM-V and -PV estimates of GPP are compared to MODIS (MOD17A2H) GPP product and AmeriFlux eddy covariance outputs of GPP. We also compare DCHM estimates of ET to AmeriFlux eddy covariance flux tower estimates by dividing observed latent heat flux by the latent heat of vaporization of water ($\lambda_w = 2.5$ MJ kg^{-1}, Dingman, 2015)).

185 **2.4 Description of Study Sites**
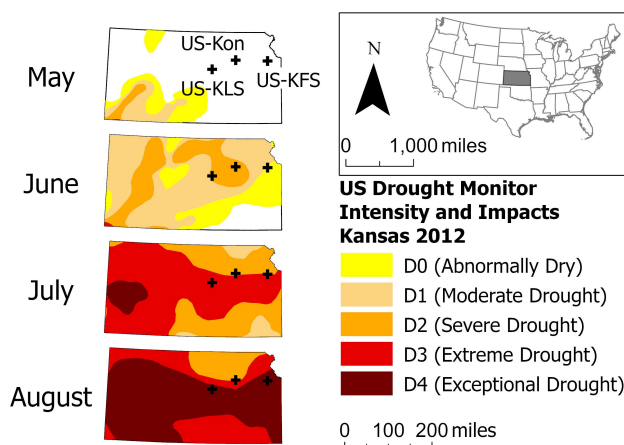
Figure 2. Evolution of the 2012 flash drought from May - August in the US Drought Monitor with the three AmeriFlux tower study sites (US-KFS, US-KLS, and US-Kon).

This study focuses on three AmeriFlux sites in Kansas (US-KFS, US-KLS, US-Kon, Figure 2 and Table 2), chosen because of the availability of GPP and latent heat (converted to ET) data during the flash drought year of 2012 and at least one wet year after 2012. When available, we used gap-filled FLUXNET FULLSET data for US-KFS and US-Kon (Pastorello et al., 2020). All three sites are classified as grasslands according to the International Geosphere-Biosphere Programme (IGBP) land cover

190 and all three sites have Cfa (humid, subtropical) Köppen Climate Classifications (Brunsell, 2020a, 2021, 2020b). US-KFS is located within a grassland-deciduous forest boundary area and receives 1014 mm of precipitation annually (Brunsell, 2020a). US-KLS is a perennial agricultural study sties receiving 812 mm of rainfall each year (Brunsell, 2021). US-Kon is part of the Konza Prairie Long-term Ecological Research (LTER), recieves 867 mm of precipitation, and is burned annually. Static

characteristics of PFT, soil texture and porosity, and geographic information for the study sites are shown in Table 2. According
195 to the MODIS land cover classification product (MCD12Q1), each site had a unique vegetation cover type (savanna, grassland,
cropland, Table 2). The PFT is a result of interpolating MODIS MCD12Q1 Land Cover Type 2 to the 4-km grid and does not
align with the land cover from AmeriFlux in all cases. The soil texture and porosity are interpolated CONUS-Soil (Miller and
White, 1998) values.

Table 2. AmeriFlux study sites contained within Stage-IV pixels.

Site	Latitude	Longitude	PFT	Soil Texture	Soil Porosity	Mean Precipitation [mm yr^{-1}]	Reference
US-KFS	39.0561	-95.1907	SAV	silty clay loam	0.4225	1012	Brunsell (2020a)
US-KLS	38.7754	-97.5684	CRO	silt loam	0.4812	812	Brunsell (2021)
US-Kon	39.0824	-96.5603	GRA	silty clay loam	0.4588	867	Brunsell (2020b)

Plant functional type (PFT), soil texture, and soil porosity determined after interpolation to the Stage-IV grid. Abbreviations: SAV = Savanna, CRO = Cropland, GRA = grassland. Precipitation totals listed as AmeriFlux annual mean.

2.5 Description of Modeling Work

200 ### 2.5.1 Land-Surface Hydrology Model

We employ two 1-D versions of the DCHM coupled land-surface hydrology model that accounts for water and energy
exchanges between three soil layers, the surface, and the atmosphere (Lowman and Barros, 2018, 2016; Tao and Barros,
2014, 2013; Yildiz et al., 2009; Yildiz and Barros, 2007, 2005; Gebremichael and Barros, 2006; Garcia-Quijano and Barros,
2005; Devonec and Barros, 2002; Barros, 1995). A 4-km grid resolution and 1-hr timestep were chosen to run the model to
205 match the native spatial resolution of the Stage-IV precipitation data, as precipitation is the main source of uncertainty when
modeling drought (Trenberth et al., 2014). We use 80 mm for the top layer soil depth to ensure model stability, but middle
and deep layers were selected to best match the USDA Kansas soil profile (Soil Survey Staff). This yields three soil layers:
top (0-80 mm), middle (80-890 mm), and bottom (890-1830 mm). Rooting depth and density, which are used to determine the
total root water uptake in the DCHM, are calculated using empirical exponential root distribution functions that vary by PFT
210 (Lowman and Barros, 2016; Zeng, 2001; Lai and Katul, 2000; Jackson et al., 1996; Clausnitzer and Hopmans, 1994). Soil layer
and rooting depths align with the different combinations of soil textures and PFTs found in Thornthwaite and Mather (1957).

The DCHM water balance includes subroutines for evaporation from the different components of the land surface (i.e.,
bare soil, and vegetation), ponding and groundwater runoff, snow accumulation and melt, and root water uptake while energy
balance routines solve for net radiation, and sensible, latent heat, and ground heat fluxes (Lowman and Barros, 2018, 2016; Tao
215 and Barros, 2014, 2013; Yildiz and Barros, 2007, 2005; Garcia-Quijano and Barros, 2005; Devonec and Barros, 2002; Barros,
1995). The water and energy balances both influence photosynthesis, which is simulated using the Farquhar model (Lowman
and Barros, 2016; Garcia-Quijano and Barros, 2005; Farquhar and Caemmerer, 1982; Farquhar et al., 1980).

2.5.2 Predictive Phenology

The key difference between the two versions of the DCHM used for this study is that within the DCHM-V vegetative phenology is forced using the MODIS MOD15A2H FPAR and LAI products, while the DCHM-PV predicts phenology for the next day based on the current day conditions. Establishing differences in the outputs from DCHM-V and -PV illuminates changes in plant growth strategies. MODIS is a passive sensor and uses only the red (648 nm) and near-infrared (NIR, 858 nm) spectral bands to estimate values of LAI (Myneni et al., 2015). Within the DCHM-PV, the dynamic canopy biophysical properties (DCBP) model predicts plant life stage based on climatological properties of water availability, air temperature, and evaporative demand (Lowman and Barros, 2018). FPAR and LAI are dynamically estimated instead of forced using MODIS observations to evaluate impacts on estimates of ET and GPP (Lowman and Barros, 2018; Kim et al., 2015; Caldararu et al., 2014).

The DCBP is the predictive phenology model that determines future plant growth based on differences between current and potential phenological states. The growing season index (GSI) determines potential phenological state based on current climate conditions (Jolly et al., 2005; Stöckli et al., 2008). Specifically it is a function of temperature, photoperiod, soil water potential, and VPD (Lowman et al., 2023; Lowman and Barros, 2018). Lowman and Barros (2018) adapted the framework to incorporate soil water parameters that affect predictions of plant growth stage. The DCBP is implemented within the DCHM-PV to estimate phenologic state with the land-surface hydrology model. However, to do this, we must first estimate parameters that determine plant growth rates and sensitivity to meteorological and soil conditions.

A Bayesian hierarchical approach is used to estimate the parameters for the DCBP. Specifically, a dual state-parameter ensemble Kalman filter (EnKF) is used to jointly estimate the phenologic states of FPAR and LAI and the eleven other parameters within the DCBP (Table 4 Lowman et al., 2023; Lowman and Barros, 2018). This method was described by Moradkhani et al. (2005) as a way of simultaneously predicting states and parameters in hydrologic models, and later implemented by Stöckli et al. (2008) to assimilate remotely sensed observations of LAI and FPAR into a predictive phenology model.

The parameter estimation procedure first consists of creating a prior distribution by sampling each state and parameter from a Gaussian distribution. This generates N=2000 ensemble members. Phenological states and input parameters are updated at every timestep for the duration of the data assimilation period using the EnKF. We assimilate MODIS LAI and FPAR every 8 days (the native MODIS temporal resolution) to reduce error and ensure phenological state predictions do not stray too far from observations (Lowman et al., 2023; Lowman and Barros, 2018).

2.6 Model Simulations

We run both the DCHM-V and -PV from 2002-2019 at a 1 h timestep and 4 km spatial resolution, spinning-up 2002 three times to allow for model stabilization (Lowman and Barros, 2016, 2018). The DCHM-V simulations provide a baseline for changes in water, energy, and carbon exchange using forced phenology from MODIS while the DCHM-PV simulations implements a predictive phenology scheme allowing us to investigate how dynamic changes in plant growth strategy impact the aforementioned fluxes.

In order to run the DCHM-PV, we first generate phenology model parameters for the predictive phenology routine. Specifically, we use 2003 (DRY), 2005 (WET), and 2003-2005 (3YR), as the data assimilation periods in the DCBP to generate parameters that correspond to wet, dry, or average precipitation regimes (Table 3). We use three different assimilation periods in order to capture the sensitivity of phenology model parameters to the meteorological conditions. It has been shown under varied climatological conditions plants can be highly adaptable, transitioning from isohydric to anisohydric in a single season (Guo et al., 2020). Lowman and Barros (2018) showed that assimilation period can determine the water stress adaptations for the modeled vegetation state. Broadly speaking, vegetation model parameters predicted using data from years with minimal rainfall represent plants accustomed to drier conditions, and therefore, they would exhibit more regulation in their water-use tendencies (Lowman and Barros, 2018; Sade et al., 2012).

To incorporate uncertainty from the phenology parameter estimation step into the DCHM-PV simulation, we run the model as Monte Carlo simulations with N=2000 members. Each ensemble member is sampled from a Gaussian distribution using the final mean and standard deviation of the parameter estimates from each of the assimilations period. In our results, we focus on analyzing model output from 2006-2019 to omit from our analysis the 2003-2005 period used in the data assimilation step.

Table 3. Summary of precipitation conditions during data assimilation periods.

Year(s)	Assimilation Period*	Stage-IV Annual Precipitation [mm yr^{-1}]		
		US-KFS	US-KLS	US-Kon
2003-2005	3YR	1066	770	847
2003	DRY	804	756	670
2005	WET	1242	806	956

*The data assimilation periods: 3YR represents a period with average annual precipitation, WET and DRY are periods with above and below average annual precipitation, respectively.

2.7 Analysis of Model Outputs

In this manuscript, we are interested in exploring whether land-surface, subsurface, and atmospheric interactions are distinct in flash drought compared to drought and non-drought periods. We focus on results from the three AmeriFlux sites for 2012 (flash drought), 2018 (drought), and 2019 (non-drought) to draw conclusions about plant response during flash drought and how they differ from drought and non-drought years. We evaluate model outputs from 2006-2019 to assess the differences between the DCHM-V and DCHM-PV model configurations during drought and non-drought years compared to a flash drought year. During this time period, we identified drought years as 2006, 2011, 2013, 2014, 2018 and non-drought years as 2007-2010, 2015-2017, 2019 using the USDM for the Central and East Central Kansas climate regions (Svoboda et al., 2002). Drought years were determined by whether parts of the region reached the D2 "Severe Drought" classification or higher. When computing drought and non-drought averages, we use the years listed here. In many time series results, we display the water year (April-October) rather than the entire year because plants are largely dormant outside of the water year in a temperate

region (Dai et al., 2016; Wang et al., 2003; Towne and Owensby, 1984). Transpiration is calculated from total root water uptake through the three soil layers, and total evaporation is computed from summing evaporation from ground and canopy surfaces, allowing us to partition ET into evaporation and transpiration (Lowman and Barros, 2018; Lai and Katul, 2000). Water-use efficiency is represented as the ratio of GPP and ET (WUE = GPP/ET, Beer et al. (2009)). We highlight differences between the DCHM-V and DCHM-PV model simulations and compare outputs to remotely sensed and in situ observations where available.
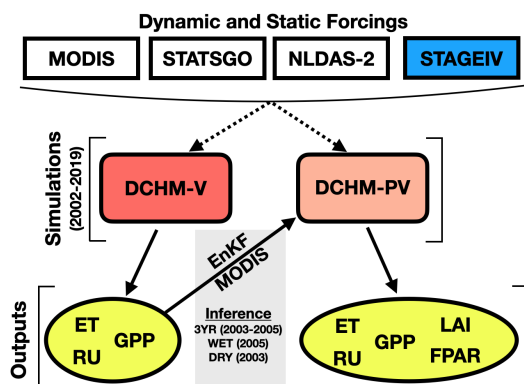
Figure 3. Schematic of modeling workflow. Spatial and temporal resolutions of all forcing data are interpolated to match the resolution of the Stage IV precipitation (4 km and 1 h), which is the resolution used for the DCHM in this study. Land cover, soil properties, and atmospheric forcing inputs come from MODIS, STATSGO, and NLDAS-2, respectively. Simulations were run from 2002-2019. We generated ensembles of parameters for three different precipitation regimes: 2003 (DRY), 2005 (WET), and 2003-2005 (3YR) for the predictive phenology routine in the DCHM-PV. The data assimilation procedure used an ensemble Kalman filter (EnKF) with simulated soil water potential and vapor pressure deficit from the DCHM-V, MODIS MOD15A2H FPAR/LAI, and concurrent meteorological conditions. The DCHM-V outputs of interest included evapotranspiration (ET), root water uptake (RU), and gross primary productivity (GPP). Additional DCHM-PV outputs included predicted fraction of photosynthetically active radiation (FPAR) and leaf area index (LAI).

3 Results

3.1 Phenology

3.1.1 Growth Rate Parameter

The growth rate parameter, γ, dictates how much phenological state (i.e. FPAR and LAI) can change in a given time step (Lowman and Barros, 2018; Stöckli et al., 2008). The uncertainty in γ shows the variability in vegetation responses to changing phenological states. Lower uncertainty in γ establishes the 3YR assimilation period, with a mixture of wet and dry years, as the preferred choice for running the DCHM-PV (Figure 4). This finding is in agreement with Lowman and Barros (2018) who found that using assimilation periods with both wet and dry conditions has the effect of capturing adaptive plant water-

use strategies. This lower uncertainty propagates through the DCBP in the DCHM-PV, leading to lower uncertainty in the predictions of FPAR and LAI (Figures 5 and 6). The values of γ vary by site due to a combination of local climate and vegetation type. US-KFS, modeled as a savanna, has the lowest mean and standard deviation of γ (Table 4). The smaller magnitudes of the growth parameters indicates that vegetation is less likely to make abrupt changes and exhibit more resilience when faced with extreme dry down. Other parameter estimation outputs used to generate ensembles from the 3YR assimilation period can be found in Table 4.
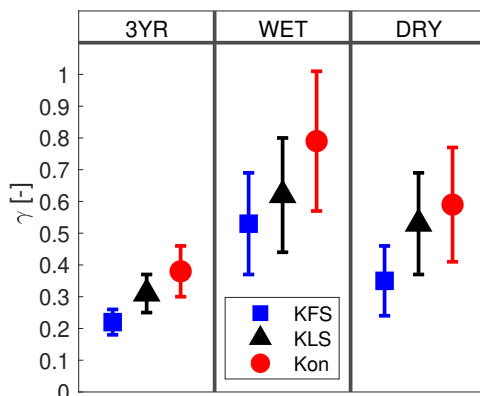
Figure 4. Ensemble means and one standard deviation of the growth rate parameter, γ [-], for each site and all three data assimilation periods: 3YR (2003-2005), WET (2005), DRY (2003).

3.1.2 Fraction of Photosynthetically Active Radiation

Overall, DCHM-PV simulated FPAR tends to follow the same patterns as MODIS throughout the growing season, irrespective of choice of parameters. Results indicate slower senescence and reduced variance using the 3YR assimilation parameters as compared to the WET and DRY parameters during late June and early July 2012 across all three sites (Figure 5a, d, g). This aligns with the known period of flash drought that occurred across Kansas (Lisonbee et al., 2021). The predicted values of FPAR at US-KFS and US-KLS are slightly higher than the MODIS values during the 2012 growing season. The predicted values of FPAR match well against MODIS for the US-Kon site, especially during the decline in late June through July. During the flash drought period, there is a notable decrease in variance, or uncertainty, across the Monte Carlo simulations.

For US-KFS across the three simulations, the simulation using the WET parameters achieves a higher FPAR during the flash drought and holds its peak throughout the month of May, with declines beginning in June and bottoming in early July before rising again in the latter part of the growing season. FPAR decreases from 0.77 to 0.41 for the WET parameters while reductions from the time of peak FPAR to early July in the simulations using DRY and 3YR parameters are from 0.73 to 0.47 and 0.76 to 0.53, respectively. The decreases in FPAR observed from mid-May to mid-July in 2012 are more pronounced than during the growing season of the drought year 2018 when fluctuations in FPAR were smaller. Results from an above average precipitation year (2019) show a steady increase, a longer peak growing season, and a decrease in line with fall

Table 4. Ensemble mean and one standard deviation of predictive phenology model parameters from the 3YR assimilation period

Parameter	Description	Units	Mean parameter estimates ± one standard deviation		
			US-KFS	US-KLS	US-Kon
$T_{min_{min}}$	minimum value of daily minimum temperature	°C	-5.5 ± 3.1	0.1 ± 2.4	-2.3 ± 3.2
$T_{min_{max}}$	maximum value of daily minimum temperature	°C	14.0 ± 1.8	16.5 ± 1.8	15.8 ± 2.0
Pht_{min}	minimum daily exposure to sunlight	h	10.0 ± 0.4	9.8 ± 0.6	10.7 ± 0.6
Pht_{max}	maximum daily exposure to sunlight	h	14.3 ± 0.3	14.2 ± 0.4	14.3 ± 0.4
$VPD_{avg_{min}}$	minimum daily average vapor pressure deficit	mb	17.1 ± 1.3	16.6 ± 1.4	16.9 ± 1.4
$VPD_{avg_{max}}$	maximum daily average vapor pressure deficit	mb	58.7 ± 2.3	55.8 ± 2.2	55.6 ± 2.3
$\psi_{soil,avg_{min}}$	minimum daily average soil water potential	J kg^{-1}	-42.1 ± 5.6	-37.2 ± 5.8	16.9 ± 5.5
$\psi_{soil,avg_{max}}$	maximum daily average soil water potential	J kg^{-1}	-7.4 ± 1.3	-7.0 ± 1.4	-6.9 ± 1.4
$FPAR_{min}$	minimum fraction of photosynthetically active radiation	-	0.31 ± 0.01	0.35 ± 0.01	0.31 ± 0.01
LAI_{max}	maximum leaf area index	m^2 m^{-2}	6.36 ± 0.15	6.51 ± 0.17	6.65 ± 0.18
γ	growth rate	day^{-1}	0.22 ± 0.04	0.31 ± 0.06	0.38 ± 0.08

For an in depth description of the predictive phenology routine within dynamic canopy biophysical properties (DCBP) model see Lowman et al. (2023) and Lowman and Barros (2018).

senescence across all simulations. However, using WET and DRY parameters at US-KLS lead to ~0.2 reduction in FPAR in July 2019, opposed to ~0.1 reduction from the 3YR parameters. The larger reduction is likely due to the below average July precipitation and the larger WET and DRY values of γ leading to more rapid phenological changes. Similar to the 2012 results, 2019 simulations using phenology parameters from the 3YR assimilation period showed slower late-season declines in FPAR than simulations using parameters from the WET or DRY assimilation periods. This can be seen from the 3YR parameter simulations for US-KLS and US-Kon which show higher FPAR through July.

3.1.3 Leaf Area Index

Predicted values of LAI are similar to MODIS LAI with small relative differences (Figure 6). During the flash drought year of 2012, a steep decline in modeled LAI can be seen in late June and early July across the three sites. LAI declines almost 1 m^2 m^{-2} in a few weeks during summer 2012 compared to steadier values during the drought of 2018. Growing season LAI was ~0.5 m^2 m^{-2} lower in 2012 compared to 2018. The DCHM-PV model outputs of LAI during 2019 match MODIS but are 1-2 m^2 m^{-2} higher during June, July, and early August at US-KFS and US-KLS, and slightly lower than MODIS at US-Kon.

Simulated LAI values vary slightly across the three sites. For US-KFS, simulations using the WET year parameters achieve higher values in LAI than the other two simulations (Figure 6a-c). For US-KLS, and US-Kon, the growing season LAI has the highest peaks in the simulations using the 3YR parameters (Figure 6d-i). With more rainfall in May and June 2019, the simulations using the WET parameters result in lower LAI than the simulations using the DRY parameters.
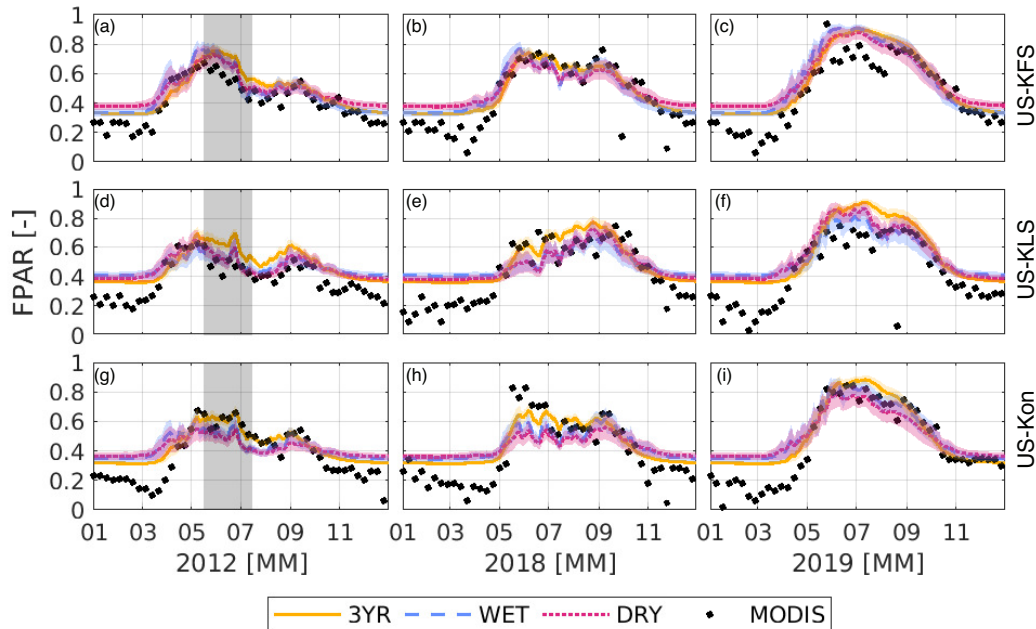
Figure 5. Fraction of photosynthetically active radiation, FPAR [-], predicted from the DCHM-PV for the flash drought year (2012), a drought year (2018), and a non-drought year (2019) for US-KFS (top row), US-KLS (middle row), and US-Kon (bottom row). Colors indicate the different data assimilation periods: 3YR (yellow), WET (blue), DRY (red). Corresponding shaded regions represent one standard deviation of model outputs from the 2000 ensemble members. The 8-day MODIS MOD15A2H FPAR is shown as black dots. The gray shaded regions in the left most panels highlights the 2012 flash drought period.

325   The most consistent similarities across the phenology results is that the simulations using the 3YR parameters generally show a slower decline in LAI in flash and non-flash drought years for all sites. Additionally, the simulations using WET and DRY parameters are more similar to each other than to the simulations using 3YR parameters. This result is commensurate with the values of the means and variances of γ resulting from the different assimilation periods. Simulations using the 3YR assimilation period result in LAI remaining high for a longer period of time with a decrease in response to flash drought

330   developing slower than the other two simulations. This is also apparent for US-KLS and US-Kon in the 2019 3YR simulations in which leaf growth continues through June and peaks in the middle of July, while in the WET and DRY simulations new growth tends to slow from the beginning of June through mid-July.

   Generally, the predictive phenology model compares favorably with the seasonal changes observed in MODIS FPAR and LAI (Figures 5 and 6) in both flash drought and non-flash drought periods. In the summer, at US-KFS and US-KLS during

335   2019, the model tends to predict FPAR and LAI values higher than MODIS. In 2019, at US-KFS, MODIS observed a steady decline in FPAR from 0.8 to 0.6 throughout July followed by an increase to 0.8 over an 8-day period at the beginning of August (Figure 5c). The DCHM-PV results do not show the same decline. Similarly, MODIS observes a drop in LAI before an abrupt
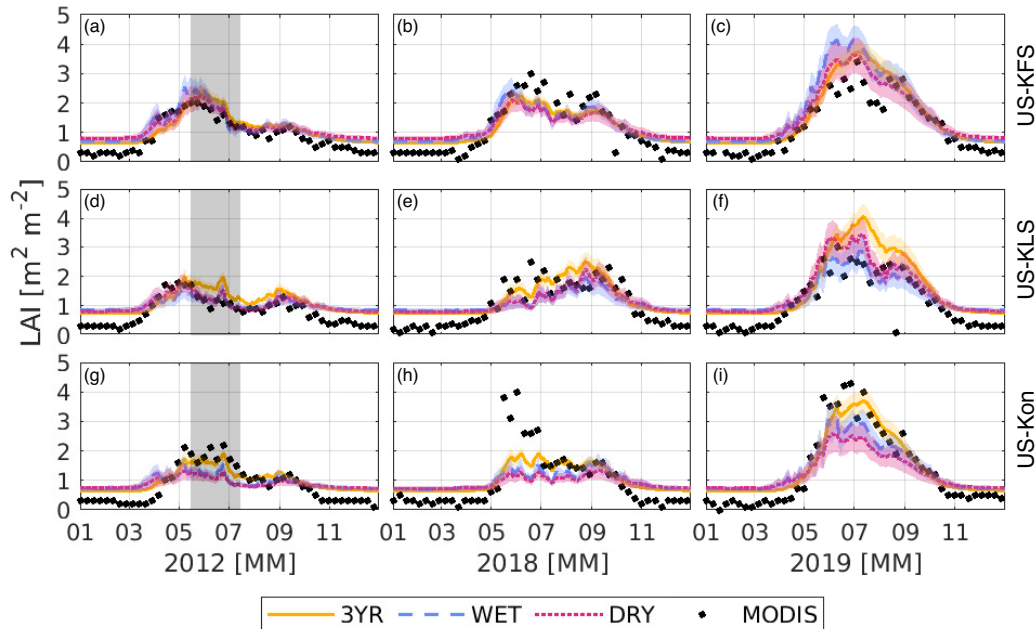
Figure 6. Leaf area index, LAI [$m^2 \, m^{-2}$], predicted from the DCHM-PV for the flash drought year (2012), a drought year (2018), and a non-drought year (2019) for US-KFS (top row), US-KLS (middle row), and US-Kon (bottom row). Colors indicate the different data assimilation periods: 3YR (yellow), WET (blue), DRY (red). Corresponding shaded regions represent one standard deviation of model outputs from the 2000 ensemble members. The 8-day MODIS MOD15A2H LAI is shown as black dots. The gray shaded regions in the left most panels highlights the 2012 flash drought period.

increase while model estimates remain higher than MODIS (Figure 6c). Yet, in June 2019 at US-Kon, the DCHM-PV estimates are lower than MODIS LAI.

340   The bulk of the following results and analysis compares vegetation responses during flash drought and non-flash drought periods rather than an inter model comparison across the different assimilation strategies. Estimates from the WET and DRY simulations tend to be in agreement with results from the 3YR simulations. From this point forward, we only show results from the 3YR simulations.

3.2   Sub-surface Water

345   **3.2.1   Infiltration**

During non-drought years, monthly infiltration accumulations are above or near 100 mm per month, on average, from April to July with the highest amounts in May (Figure 7). During drought years, infiltration between April-July is less than non-drought years. Furthermore, monthly accumulated infiltration is lower during the flash drought year compared to both drought and non-drought years, suggesting there is less water available for plant use during the growing season. At US-KFS from April-October
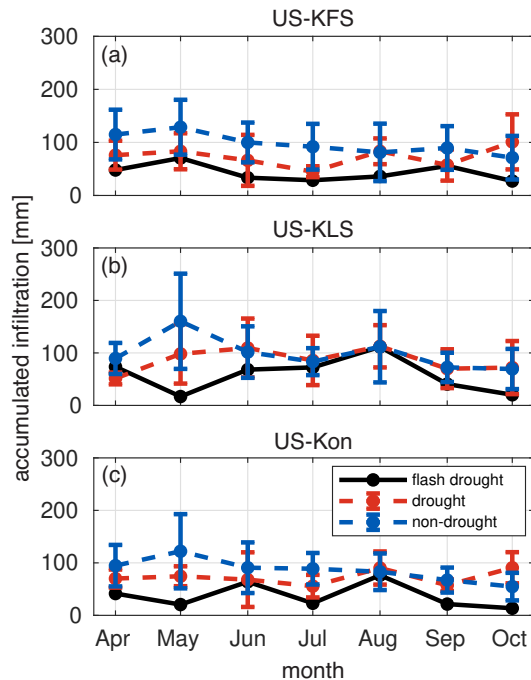
Figure 7. DCHM-PV 3YR ensemble means of monthly infiltration accumulations [mm] for drought (red) and non-drought (blue) years compared to 2012 (black) for US-KFS (top), US-KLS (middle), and US-Kon (bottom). Monthly sums are computed from the ensemble means of the 2000 Monte Carlo simulations then averaged across drought or non-drought years. Error bars represent one standard deviation across drought and non-drought years.

350   of 2012, monthly infiltration is slightly below what is observed during drought years. A large decline in May infiltration at US-KLS and US-Kon led to infiltration accumulations 1-2 standard deviations below average drought conditions. All sites had infiltration rates below 100 mm for all months during 2012 with the exception of US-KLS in August 2012.

Low monthly infiltration amounts during the flash drought year are likely due to lower precipitation accumulations, coupled with an increase in the number of days between precipitation events, and an increase in atmospheric demand for water (Figures
355   8, S4, and S5). During drought and non-drought years, the average number of days between rainfall events within a month ranges from 1 to 7 days, while the lower end for the flash drought year is higher at 2.5 days. Here, we consider a rainfall event to be any day with recorded precipitation. Additionally, during drought and non-drought years, monthly infiltration exceeds 150 mm, but in 2012 remains at or below 75 mm for all sites aside from August 2012 at US-KLS where monthly infiltration is ∼110 mm. In 2012, all three sites averaged over four days between rainfall events during May, June, and July with US-KFS
360   averaging over six days between rainfall events during both May and June and more than five days in July (Figure 8a). Across all three sites from April-October 2012, there were more than four days between precipitation events 80% percent of the time compared to just 20% of the time in non-flash drought years.
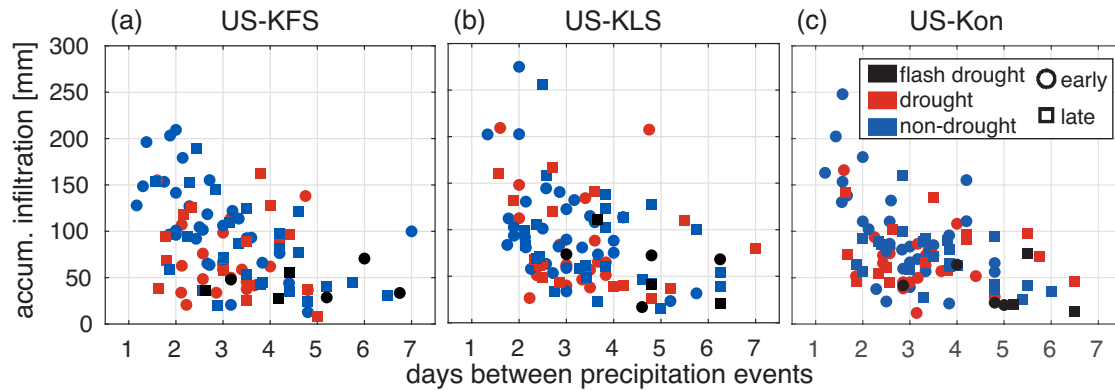
Figure 8. Monthly infiltration accumulation [mm] vs average days between precipitation events within a single month for (a) US-KFS, (b) US-KLS, and (c) US-Kon. Each shape indicates whether the month occurs in the early growing season (circle: April - July) or late growing season (square: August - October). Colors distinguish flash drought (black) from drought (red) and non-drought (blue) years.

3.2.2 Soil Moisture

Soil moisture analysis and comparison to other soil moisture products is similar for all three study sites. Figures for soil moisture at US-KFS for all three soil layers are available in supplemental material. Top layer soil moisture reaches the wilting point several times throughout the flash drought period of 2012 (Figure S1a). During peak flash drought, at the end of June and beginning of July, moisture content remains at wilting point for many days. Daily soil moisture agrees with AmeriFlux soil moisture observations in the top layer during 2012 at US-KFS. Discrepancies exist in 2018 when AmeriFlux observations fall to levels just above 0 m^3 m^{-3}.

Fluctuations in soil moisture match favorably with NLDAS-2 estimates across the top two layers in 2012, 2018, and 2019. However, middle layer soil moisture from the DCHM estimates is about 0.05 m^3 m^{-3} higher than NLDAS-2 and SMERGE by the late growing season of the flash drought year (Figure S2). The DCHM estimates remain fairly steady in the deep layer during 2012, while NLDAS-2 soil moisture estimates continue to fall throughout the rest of the growing season (Figure S3). The steady DCHM soil moisture levels during flash drought may be indicative of the modeling stunting root water uptake during the same time, preserving soil water content.

3.2.3 Root Water Uptake

Root water uptake is above non-flash drought levels in 2012 before the onset of flash drought in June. Then it remains lower than non-flash drought levels for the remainder of the growing season (Figure S6). The middle soil layer is responsible for up to four times more root water uptake than the other layers. Thus, a major decline in root water uptake through the middle layer is informative of how plant water-use is altered during drought. While root water uptake starts out in 2012 at levels above average non-drought years, it falls to more than one standard deviation below drought averages by July. This drastic shift is
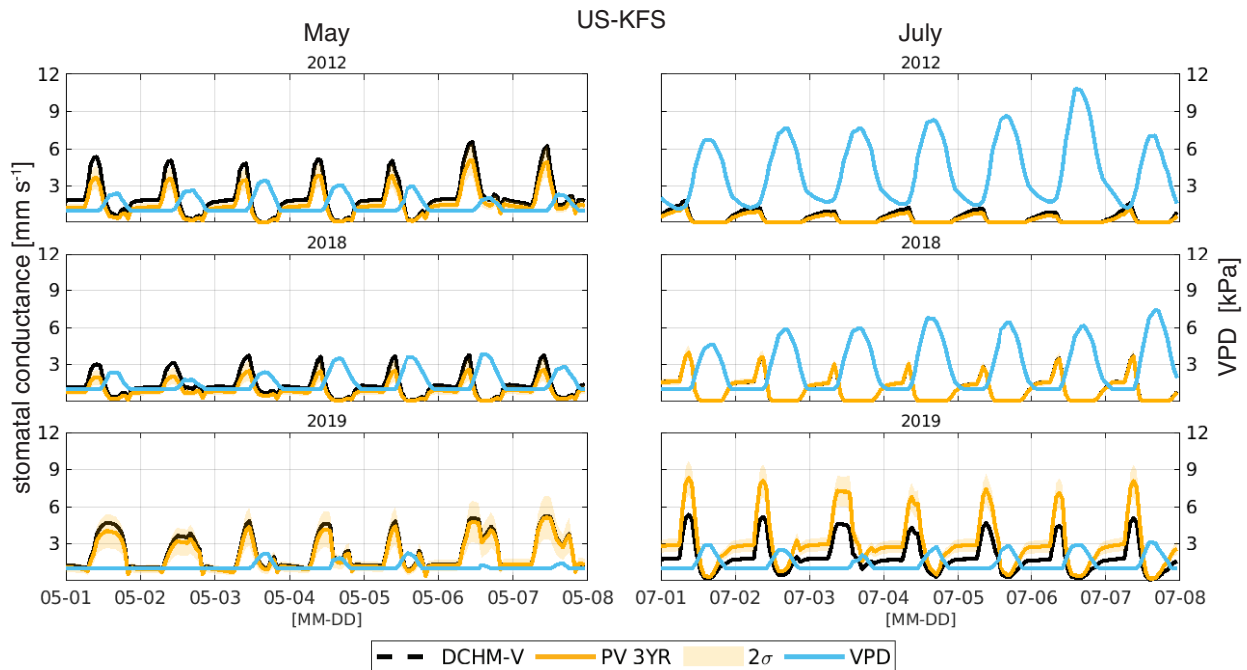
Figure 9. Stomatal conductance [mm s^{-1}] and VPD [kPa] for one week in May (left) and July (right) of 2012, 2018, and 2019 for US-KFS.

likely due to lower infiltration (Figure 7), and drives down rates of transpiration within the DCHM-V and -PV over the same period.

3.3 Plant-Atmosphere Interactions

385 #### 3.3.1 Sub-daily Stomatal Conductance

Sub-daily estimates of stomatal conductance highlight how VPD can drive stomatal activity within the DCHM. In 2012, stomatal conductance in the first week of May was as high or higher than in 2019, a non-drought year at US-KFS (Figure 9). But by July, major differences in 2012 and 2019 stomatal conductance coincide with changes to VPD. In July 2012, high VPD shuts down midday stomatal conductance whereas lower values of VPD allow for higher rates of stomatal conductance during 390 the same time in 2019. The large reduction in stomatal conductance from the first week of May to the first week of July during the flash drought year of 2012 is unlike that seen in a drought year like 2018 where stomatal conductance rates are similar in May and July.

3.3.2 Gross Primary Productivity

Monthly averages of GPP accumulations from the DCHM-PV ensemble means throughout the water year (April - October) 395 indicate carbon uptake falls below drought averages from May to June during the flash drought year of 2012 (Figure 10a, c,
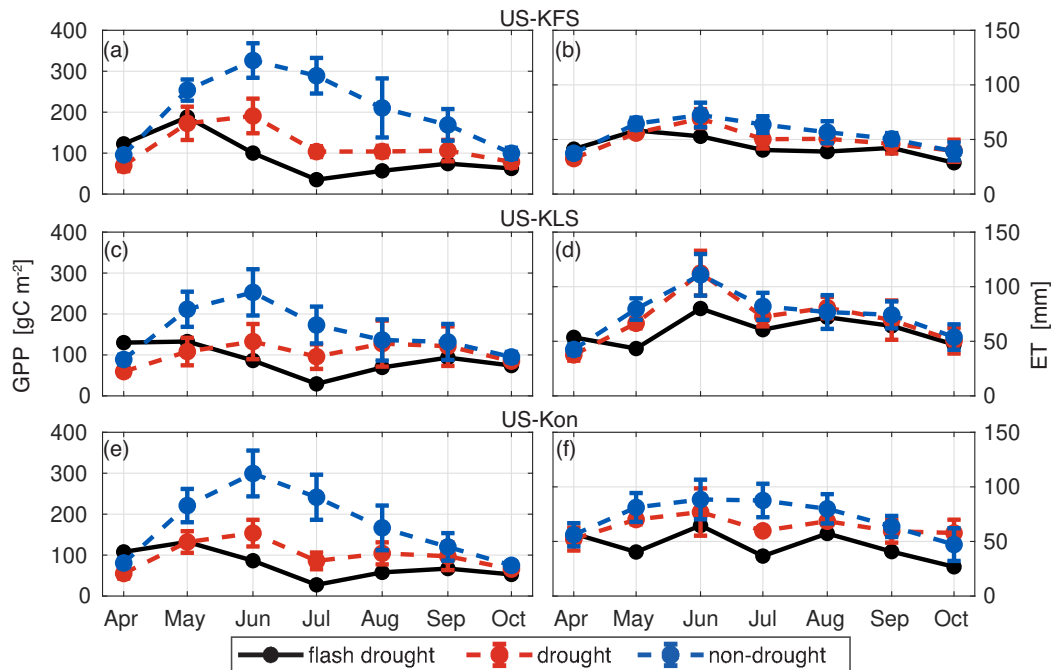
Figure 10. DCHM-PV 3YR monthly totals of GPP [gC m^{-2}] (left) and ET [mm] (right) for drought (red) and non-drought (blue) years compared to flash drought (black) for US-KFS (top row), US-KLS (middle row), and US-Kon (bottom row). Monthly totals are computed from the ensemble means of the 2000 Monte Carlo simulations then averaged across drought or non-drought years. Error bars represent one standard deviation across drought and non-drought years, respectively.

e). Flash drought carbon assimilation amounts remain below drought levels before converging to average drought/non-drought levels by the end of October. GPP amounts are up to 50% lower in drought years compared to non-drought years. During the flash drought, GPP monthly totals in June through August 2012 are at least one standard deviation lower than drought years averaged over the 2006-2019 simulation period. June 2012 GPP accumulations are half that of drought years and less than 30% of non-drought years. An even greater discrepancy is apparent in July with carbon assimilation amounts less than 30% of drought levels and 15% of non-drought levels. Despite increased GPP from July to August in 2012, accumulations are still one standard deviation below drought levels.

Seasonal variations of GPP at US-KFS for simulations from the DCHM-V and -PV (3YR) with observations from MODIS and AmeriFlux for the flash drought year (2012), a drought year (2018), and a non-drought year (2019) can also be explored at the daily scale (Figure 11). Daily GPP is lower in drought versus non-drought years between April and October. During the flash drought year, there is a decline in GPP from 10 gC m^2 d^{-1} in early May, above what was observed in 2018 and 2019, to near zero by July in 2012 (Figures 11, S15, and S16). During the drought year (2018), daily GPP remains low throughout the growing season, but never decreases to below 1.2 gC m^2 d^{-1} at US-KFS. From June to July in 2012, carbon uptake decreased from more than 5 to less than 1 gC m^{-2} d^{-1}. This type of decline is not observed in a drought year (e.g., 2018). The rapid
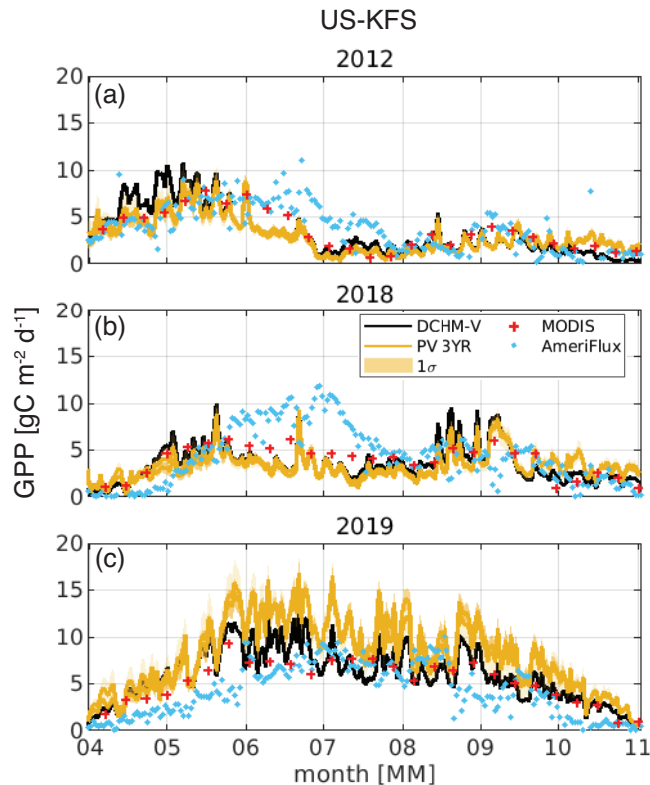
Figure 11. Daily gross primary productivity, GPP [gC m^{-2}], at US-KFS for (a) 2012 flash drought, (b) 2018 drought, and (c) 2019 a non-drought year. One standard deviation is shown as a shaded region for the DCHM-PV simulations. MODIS GPP are shown as red crosses and AmeriFlux GPP as blue dots.

410   decline in GPP from May to July is what distinguishes the 2012 flash drought as a period of time where land-atmosphere interactions switch from resembling conditions of a wetter than an average wet year to a drier than an average dry year. The DCHM-PV GPP results are similar to MODIS GPP in most cases, with the exception that it tends to underestimate GPP compared to MODIS in a drought year, aligning with the higher MODIS estimates of FPAR and LAI during the same periods (Figure 6). Simulated GPP tends to underestimate flux tower GPP during June and July in 2012 and 2018, but overestimate in
415   2019.

3.3.3   Stomatal and Non-stomatal Regulation of Gross Primary Productivity

We examine how GPP covaries during flash drought, drought, and non-drought years with sub-seasonal changes in LAI and stomatal conductance at US-KFS (Figure 12). During a non-drought year (2019), there exists a wider range of values of stomatal conductance, LAI, and GPP throughout the growing season (Figure 12c). There is a clear seasonal cycle in the
420   clockwise movement through the stomatal conductance-LAI parameter space. Stomatal conductance increases faster than LAI
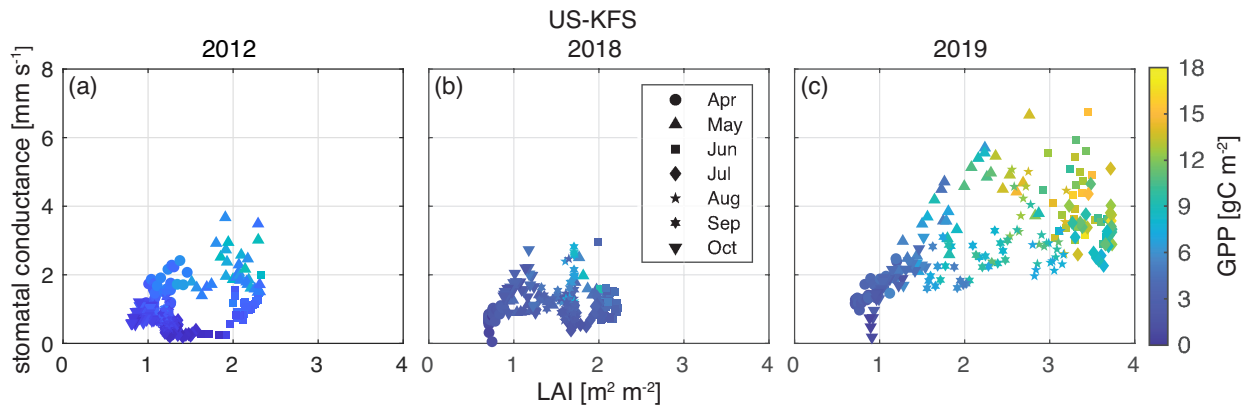
Figure 12. Stomatal conductance [mm s^{-1}] vs leaf area index, LAI [m^2 m^{-2}], for US-KFS for a flash drought year (2012), a drought year (2018), and a non-drought year (2019). Marker shapes indicate individual days between April 1 - October 31. Each month is given a unique shape whose color reflects daily accumulations of gross primary productivity, GPP [gC m^{-2}].

in the early season before reaching maximum values around June. After LAI peaks, there is first a reduction in stomatal conductance and GPP at higher LAI before LAI decreases through August and September.

In contrast, during flash drought (2012) and drought (2018), peak stomatal conductance, LAI, and GPP values at US-KFS are approximately half of 2019 values. Both stomatal conductance and LAI remain low throughout the growing season and GPP is

425 below 10 gC m^{-2} at all sites in 2012 (Figure S7). Stomatal conductance and LAI are highest in May 2012 as opposed to June and July 2019. While both 2012 and 2018 have low values of stomatal conductance, LAI, and GPP, an important difference is the near-zero stomatal conductance during June and July 2012 for a range of LAI values (1-2 m^2 m^{-2}, Figure 12) that is not observed in 2018 and other drought years (Figure S11).

The relationship between stomatal conductance, LAI, and GPP is similar across all three sites when considering flash drought

430 (Figure S7), drought (Figure S11), or non-drought periods (Figures S8, S9, and S10). The observable clockwise movement through parameter space is not as clear in flash drought and drought as compared to non-drought. In drought years, stomatal conductance from April-October averages 1.4 mm s^{-1} across all sites (Figure S11), compared to 2.3 mm s^{-1} in non drought years (Figures S8, S9, and S10), and 1.1 mm s^{-1} in flash drought (Figure S7). Peak LAI is approximately 1-2 m^2 m^{-2} higher in non-drought years relative to flash drought and other drought years. Similarly, non-drought GPP levels are approximately

435 6-8 gC m^{-2} higher than flash drought and non-drought periods.

3.3.4 Evapotranspiration

We consider monthly accumulations of ET for the flash drought year and averaged across non-flash drought years for the three study sites (Figure 10b, d, f). ET accumulations are lower in the flash drought year starting in May, particularly at US-KLS and US-Kon. Monthly ET during drought periods are slightly lower, but generally similar to non-drought at US-KFS and US-

440 KLS, indicating that ET may not be a strong indicator of drought. However, parsing ET into its components of evaporation
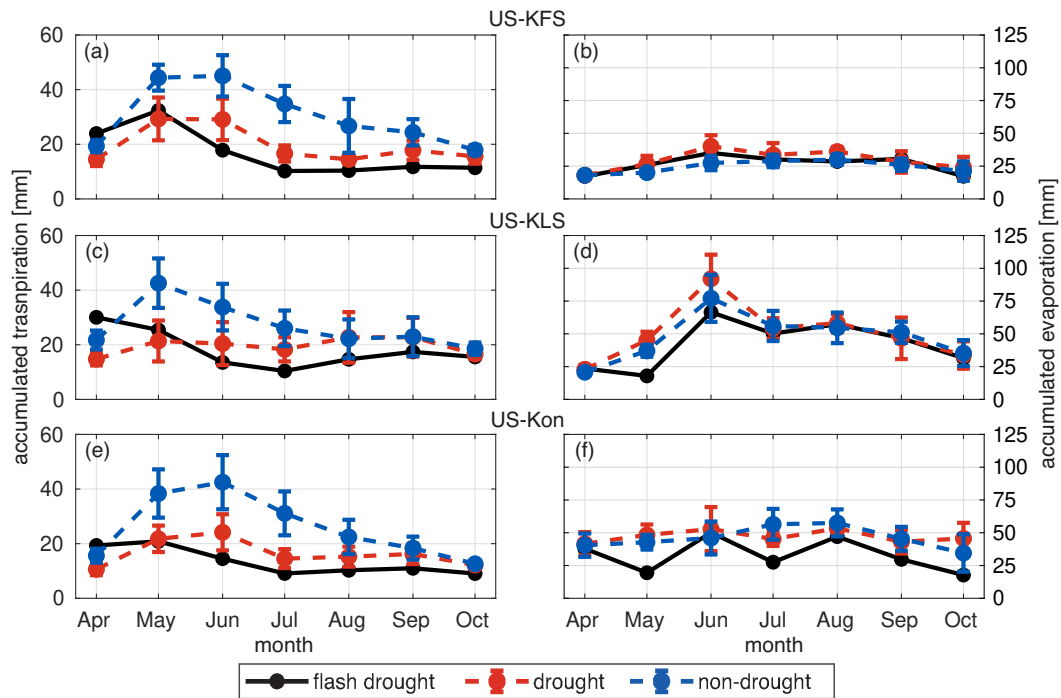
Figure 13. DCHM-PV 3YR monthly totals of transpiration [mm] (left) and evaporation [mm] (right) for drought (red) and non-drought (blue) years compared to flash drought (black) for US-KFS (top row), US-KLS (middle row), and US-Kon (bottom row). Monthly totals are computed from the ensemble means of the 2000 Monte Carlo simulations then averaged across drought or non-drought years. Error bars represent one standard deviation across drought and non-drought years, respectively.

and transpiration offers a different perspective. Simulated monthly transpiration accumulations follow trajectories similar to GPP during flash drought (Figure 13a, c, e). Transpiration amounts during flash drought exceed non-drought years in April, match what is observed during drought years in May, and decline to levels below drought years through the rest of the growing season. Transpiration in July 2012 falls below one standard deviation of the drought years. At all sites, evaporation rates for

445   drought and non-drought years are similar. At US-KFS, monthly evaporation is comparable to both drought and non-drought years throughout the entire growing season (Figure 13b). At US-KLS, May and June evaporation totals are lower during the flash drought than drought and non-drought years. At US-Kon, May and July evaporation falls below drought and non-drought years.

During the flash drought, transpiration gradually declined from May to July (Figures 13 and S19a). The fluctuations in total

450   ET starting in June 2012 are the result of evaporation in response to small precipitation events. This suggests that following precipitation events during flash drought onset, ET is dominated by evaporation. Reduced infiltration limits water available for root water uptake (Figures 7 and S6). As transpiration is computed from root water uptake across the three soil layers, the observation that transpiration decreases but maintains a small consistent rate through the flash drought indicates that vegetation is extracting water from deeper soil layers. ET never completely shuts down in 2012 because of the low rate of transpiration.

455 However, evaporation completely halts during early July 2012, which is the peak of the flash drought period. Similar to flash drought, during drought in 2018, ET is dominated by evaporation (Figure S19b). But in the non-drought year 2019, transpiration makes up more than 50% of ET throughout the entire growing season except for short periods in July and August (Figure S19c).
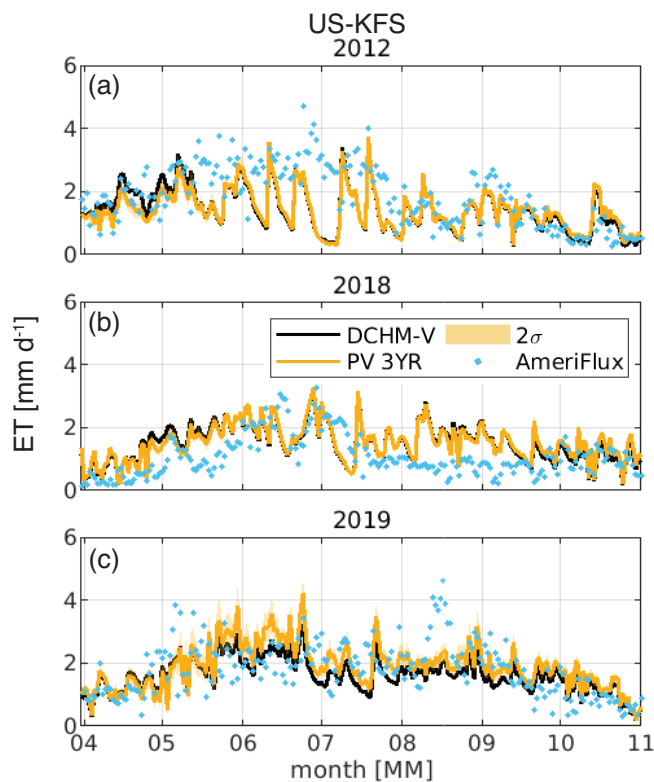
Figure 14. Daily evapotranspiration, ET, at US-KFS for (a) 2012 flash drought, (b) 2018 drought, and (c) 2019 a non-drought year. Two standard deviations are shown for the DCHM-PV simulations. AmeriFlux ET is derived from latent heat measurements and shown as blue dots.

Daily ET estimated by the DCHM-PV matches well against AmeriFlux estimates at US-KFS during the flash-drought, and non-flash drought years (Figure 14). In 2012, the DCHM-PV ET agrees with AmeriFlux through mid-May. From late May

460 through July the model results tend to fall below AmeriFlux until August when they once again agree. In the drought (2018) and non-drought (2019) years, the DCHM-PV ET appears to align with AmeriFlux throughout most of the season (Figure 14b, c). While model estimates of ET are higher than flux tower measurements in 2019 at US-KLS, they compare favorably in 2012 and 2018 (Figure S17). In contrast to model and flux tower comparisons at US-KFS and US-KLS, at US-Kon (Figure S18), modeled ET agrees with AmeriFlux in 2019 (non-drought), but underestimates during the summer months in 2012 (flash

465 drought) and 2018 (drought). One explanation for the differences between model and tower ET data could be that water-use by vegetation during flash drought is highly variable across sites, and the model is not able to represent all possible responses.

Additionally, it is difficult for the DCHM and other Earth system models to account for plant access to deep water stores (Giardina et al., 2023).

4 Discussion

4.1 Mechanisms Controlling Plant Responses to Drought

An objective of this work is to evaluate whether changes in phenology versus changes in stomatal conductance have a stronger control on carbon uptake during flash drought (H2 and H3). Prior work linked phenological responses to drought to changes in vegetation-atmosphere interactions (Lowman and Barros, 2018; Cui et al., 2017). Dynamically estimated FPAR and LAI tend to exert strong controls on the resulting GPP (Lowman and Barros, 2018). By updating phenological states using the phenology model rather than forcing phenology with remotely sensed values, we were able to capture the plant growth response to water availability. When more water is available, the DCHM-PV simulation predicts higher values of FPAR, LAI, and thus higher values of GPP. At the onset of flash drought, the DCHM-V and -PV respond faster than MODIS to changes in LAI and FPAR (Figures 5 and 6), leading to differences in modeled and remotely sensed GPP (Figure 11). Moreover, regardless of the simulation, the rapidness of the change in LAI and FPAR is indicative of flash drought, and in agreement with Zhang et al. (2020). Decreases in phenological state due to the lack of soil water available to plants affected carbon and water exchanges, suggesting support for the third hypothesis (H3), however, decreases in stomatal conductance driven by increased VPD may compound the detrimental phenological effects.

While phenology is an important component to consider when simulating changes to transpiration and carbon uptake (Lowman and Barros, 2018; Flack-Prain et al., 2019), our results indicate that stomatal conductance is also critical for accurately representing these fluxes. Plants adaptively regulate their stomata during periods of water stress (Guo et al., 2020), and some have been demonstrated to maintain open stomata or even increase stomatal conductance under high VPD conditions (Urban et al., 2017). Stomatal conductance shuts down under high VPD in the DCHM (Figure 9), which does not account for the possibility of an adaptive stomatal regulation strategy. Since GPP is directly dependent on stomatal conductance (Farquhar and Sharkey, 1982), the DCHM estimates of sub-daily GPP decrease in response to elevated VPD (Figure S22). Moreover, changes in phenological growth state (i.e. LAI) occur across longer (i.e. seasonal) time scales than stomatal regulation (Katul et al., 2001), which controls carbon and water exchange at sub-daily timescales (Guo et al., 2020).

The differences between modeled and observed GPP and ET (Figures 11 and 14) suggest that there are mechanisms controlling plant responses to drought stress not accounted for within the DCHM. For example, the DCHM could be too strict in representing the sensitivity of stomatal closure to elevated VPD for the Kansas study sites. There could be plant or climate specific VPD dependence (Grossiord et al., 2020), plants could have access to stores of water not accounted for (Giardina et al., 2023), or both. Guo et al. (2020) showed that isohydricity (i.e. stomatal regulation) exists on a spectrum and that some plants are able to move along that spectrum at sub-daily time-scales with varying environmental conditions, such as higher VPD. Given the high VPD in 2012 at our study sites (Figures S5, S28, S29, and S30), the DCHM estimated low stomatal conductance, and thus low GPP relative to AmeriFlux observations when under atmospheric water stress. This was evident in

the slow reduction in GPP during May and June 2012 before reaching a minimum near the beginning of July marking stomatal closure and a shift toward more isohydric behavior (Figures 10 and 11; Meinzer, 2002). Additionally, VPD estimated by the DCHM using the NLDAS-2 Forcing File A atmospheric variables is higher during 2012 and 2018 and lower in 2019 than the AmeriFlux observations (Figure S28), explaining in part the discrepancies between model and AmeriFlux GPP. As stomatal response to increasing VPD and resulting impacts on land-atmosphere water fluxes is more complex than how it is represented in LSMs (Vargas Zeppetello et al., 2023), future modeling studies should focus on how rising VPD drives stomatal closure across different vegetation types (Grossiord et al., 2020).

4.2 Surface and Sub-surface Water Movement

At the onset of flash drought there is an increase in evaporative demand for water which leads to a temporary increase in surface evaporation (Lowman et al., 2023; Otkin et al., 2018). Once the soil and canopy reservoirs no longer contain enough water, evaporation shuts down. Despite evaporation tapering to zero during June and July of 2012 (Figure S19), pulses of rainfall led to temporary rapid increases in rates of evaporation. Increased surface evaporation may reduce water infiltrating the soils. Across all three study sites, infiltration exceeded evaporation in the growing season in drought and non-drought years (Figures 7 and 10). During flash drought, infiltration totals were of similar magnitude to evaporation totals. Thus, a decrease in total infiltration concurrent with increased evaporation may be an indicator of flash drought.

We found that it is important to consider the partitioning of ET when studying plant responses to flash drought. Accumulated monthly averages of transpiration as a fraction of evapotranspiration (T/ET) showed a transition from at or above non-drought levels to at or below drought levels (Figure 15). Excluding 2012, growing season transpiration rates averaged more than 50% of total ET at US-KFS. This finding aligns with prior results from Hosseini et al. (2022), who used the Noah-MP LSM that also computes transpiration from root water uptake (Li et al., 2021). However, during the flash drought year, transpiration rates fell below 35% of overall ET at US-KFS (Figure 15a). Transpiration decreased by approximately $20\% - 40\%$ from May to June at US-KLS and US-Kon (Figure 15b, c). The rapid decline in transpiration rates can be attributed to the slowing of root water uptake due to the lack of available water and decreased stomatal conductance (Figures S6 and S7). It is possible that the fluctuating T/ET at US-Kon, modeled as a grassland, is indicative of an adaptation to the water stresses.

4.3 Linking Carbon and Water Fluxes

Vegetation responses to water stress are apparent through fluctuations in GPP (Zhang and Yuan, 2020; Jin et al., 2019) and ET (Chen et al., 2019). Decreases in GPP occur when plants close their stomata, limiting gas exchange, and affecting both rates of photosynthesis and transpiration. Transpiration is only one part of ET, so we must be careful not to directly link fluctuations in GPP with fluctuations in ET. Evaporation can still be high when there is little to no transpiration, but we find GPP tends to follow the same trajectories as transpiration (Figures 10, 13, S19a; Beer et al., 2009).

Despite major reductions in infiltration and fluctuations in top layer soil moisture during flash drought onset, modeled root water uptake indicated that plants were still pulling small amounts of water through their roots (Figure S6), allowing transpiration to occur, and preventing complete shut down. With the ability to tap into water stores from deeper layers (Giardina
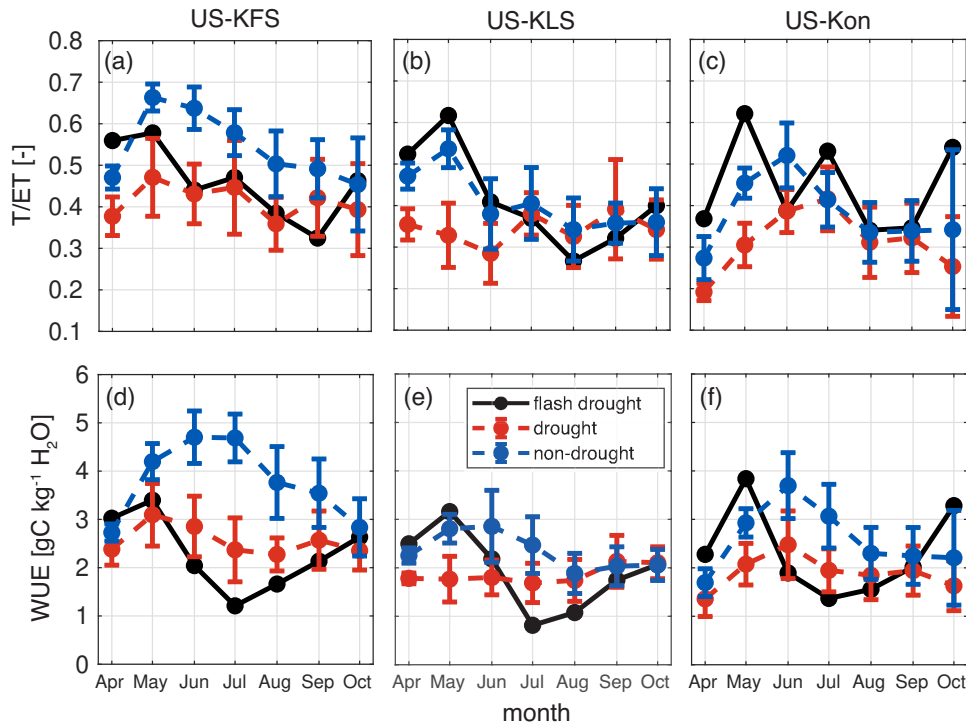
Figure 15. Ratio of transpiration to evapotranspiration, T/ET [-], and water-use efficiency, WUE [g C kg^{-1} H$_2$O], for drought (red) and non-drought (blue) years compared to flash drought (black) for US-KFS (left), US-KLS (middle), and US-Kon (right).

et al., 2023) and small rates of transpiration still occurring, modeled carbon uptake is still maintained (Figures 11a, S15a, and S16a). For example, ET decreased at US-KFS during July 2019 while experiencing a brief period of low rainfall (Figure S19b), yet plants were able to maintain rates of GPP during this period due to the amount of available water in soils from the excessive precipitation during May and June (Figures S1c, S2c, and S3c). Although GPP drastically slowed, it did not stop. The decreases in simulated GPP due to flash drought during June and July 2012 were consistent in terms of magnitude with decreases found in recent studies (Yao et al., 2022; Poonia et al., 2022; Zhang et al., 2020).

Changes to ratios of T/ET when compared with simultaneous changes in WUE indicated plants have higher rates of transpiration are more efficient in their water-use (Figure 15). We found plants are more efficient during non-drought periods, and are less efficient during flash drought onset. WUE at all sites started off in 2012 at above average non-drought levels and increased from April to May. However, from May-July, WUE at all sites fell from values above non-drought years to more than one standard deviation below drought years. With GPP differences being more substantial than ET between flash drought and non-flash drought periods (Figure 10), subseasonal reductions in WUE were attributed to the losses in GPP. Reductions in WUE from above non-drought conditions to below drought conditions. For example, the 60%-70% reduction from May to July in 2012 appeared to be a feature of flash drought onset (Figure 15d-f).

4.4 Uncertainty in Vegetation Responses

Three different assimilation strategies were used to evaluate how uncertainty propagates from the predictive phenology routine through to the DCHM-PV model outputs (Figure 3). The 2003-2005 period represented "average" conditions as it spanned periods of below and above average precipitation. Compared to the single year assimilation periods (WET and DRY), the uncertainty ranges in model parameters were smaller in the 3YR assimilation period. The results are consistent with Lowman and Barros (2018) in that uncertainty in phenology shrank during dry periods. Future studies should use an assimilation period encompassing multiple precipitation regimes (i.e. multi-year inference period) to best represent the variability of climatological conditions because it leads to reduced uncertainty in model outputs. However, if the intent of a future study is to investigate vegetation responses to extreme events in a changing climate (Kirono et al., 2020; Pearson et al., 2013, e.g.,), it may be appropriate to use inference periods encompassing extreme wet or dry conditions. For example, one could fit parameters to a dry regime to investigate how plants accustomed to today's average conditions will function in a future climate where drier conditions are expected.

The γ parameter values, which drive plant growth in the DCHM-PV, were lower in the 3YR assimilation period for all three test sites when compared to simulations from drought and wet years. Daily standard deviations in LAI across simulations were approximately 0.5 $\text{m}^2 \text{ m}^{-2}$ during the growing season of a wet year but shrank to values of 0.2 at the onset of flash drought and less than 0.1 during peak flash drought. The lower ensemble spread during the flash drought period corresponded with winter phenological variability when plants are dormant. Similarly, decreases in uncertainty in estimates of GPP and ET during the flash drought period fell to winter levels implying variability in plant life stage and functionality are similar in drought periods and dormant months.

4.5 Model Performance and Limitations

Our modeling approach permits direct comparisons of remotely sensed and ground observations to physically derived estimates. But, it should be noted that when analyzing the DCHM outputs against remotely sensed and eddy covariance measurements, we are comparing data across temporal and spatial scales. The flux towers exist within a 4 km by 4 km region defined by the Stage-IV spatial grid cell used in the DCHM. Flux tower spatial extents range from a couple hundred meters to a few kilometers (Baldocchi, 2003; Schmid, 1994), making the 4 km grid cell near the maximum range. Sub-grid scale heterogeneity can lead to considerable discrepancies between parameterized and actual fluxes (Schmid, 1994). One explanation for why flux tower data differs from model output is that the flux tower estimates incorporate a variety of vegetation types within the fetch contributing to the vertical fluxes, rather than the single vegetation type used within the model. Additionally, the size and orientation of the contributing fetch varies in time depending on measurement height and turbulent fluxes (Chu et al., 2021). Differences between model outputs and remote sensing observations could be due to discrepancies in land cover classification, a result of interpolating MODIS land cover at 500 m to the 4 km grid cell used in the DCHM. Regardless of the classification differences, the spectral reflectance method used by MODIS is inherently different from the predictive phenology routine used

in the DCHM-PV, specifically in that it cannot account for how soil water availability influences vegetation growth (Lowman and Barros, 2018).

Regardless of vegetation type, the physically-based DCHM-PV compares favorably against MODIS LAI during flash drought and non-drought at US-KFS and US-KLS and underestimates those sites during drought (Figure 6). The higher DCHM-PV model estimates of FPAR and LAI during summer 2019 could be due to the model accounting for excess water availability and other meteorological conditions favorable for growth (temperature, VPD, etc.). In contrast, MODIS estimates of FPAR and LAI are based on radiative transfer models using bidirectional reflectance of incoming radiation from the red and near infrared bands (Myneni et al., 2015; Yan et al., 2016). Our model performance against MODIS is similar to that found in Hosseini et al. (2022), who also used a predictive phenology model coupled with Noah-MP.

Daily GPP from the DCHM tends to match the magnitude of MODIS and AmeriFlux GPP at US-KFS throughout much of the growing season but underestimates June and July observations in 2012 (flash drought) and 2018 (drought). MODIS GPP is directly dependent on observations of FPAR (Running et al., 2015), and generally, MODIS overestimates GPP compared to EC flux tower data (Heinsch et al., 2006; Running et al., 2004). However, AmeriFlux estimates of GPP during June and early July of 2012 and 2018 are above estimates from MODIS. This suggests that during drought and flash drought, plants are able to maintain higher levels of GPP than what can be recreated in land surface models and satellite remote sensing. In some cases, vegetation can reallocate already processed carbon to their roots when under drought stress mitigating GPP losses (Ingrisch et al., 2020). However, differences in the DCHM-PV and AmeriFlux GPP cannot be fully attributed to carbon reallocation since the Noah-MP model accounts for carbon reallocation and similarly underestimated GPP compared to flux tower data (Hosseini et al., 2022). The DCHM-PV, which does not account for carbon reallocation, responds to drought and flash drought differently than what is observed at flux tower sites. It matches better with AmeriFlux data during 2012, the flash drought year, at US-KFS and US-KLS compared to 2018, a drought year (Figures 11 and S15).

Another explanation for the discrepancies between modeled and flux tower data could be that models may not be able to fully represent how vegetation can maintain transpiration by accessing groundwater or deep soil moisture, ultimately biasing models towards more severe effects of drought on vegetation (Giardina et al., 2023). The DCHM has similar soil moisture profiles to NLDAS-2, derived from Noah-LSM, and Hosseini et al. (2022) who used Noah-MP configurations, for both the 2012 flash drought and the 2018 drought. The DCHM estimates of GPP are often less than 50% of AmeriFlux GPP in 2012 and 2018. The model results from the Noah-MP similarly underestimate GPP and overestimate soil moisture during these drought periods (Hosseini et al., 2022), suggesting that access to deep water reserves could be responsible for these differences (Giardina et al., 2023).

4.6 Implications for Land-surface Models

Capturing phenological responses and subsequent changes to carbon and water fluxes within a physically based model is not without its limitations. Assimilating plant phenology into land-surface models (e.g., DCHM-V or Noah-MP) can improve estimates of GPP and ET (Hosseini et al., 2022; Xu et al., 2021; Mocko et al., 2021; Kumar et al., 2019). However, our findings indicate that improved phenology cannot alone account for vegetation adaptations to water stress, including the ability to access

water in ways that current LSMs cannot (Giardina et al., 2023). Future studies would benefit from improved estimates of root water uptake since it is directly linked to the amount of available water for transpiration. An emphasis should be placed on understanding how plants are able to tap into different stores of water to continue exchanging water and carbon despite lower precipitation or increased VPD. Additionally, stomata control the movement of water and carbon, affecting GPP and water-use efficiency (Lawson and Vialet-Chabrand, 2019). Sub-daily scale stomatal conductance reduces to zero in response to increased VPD leading to similar reductions in modeled GPP (Figures 9 and S22). This limitation of the the DCHM could explain why AmeriFlux GPP tends to be higher than the modeled GPP. Accounting for growing season adaptations to regulate stomatal sensitivity to drought stress as observed by Guo et al. (2022), may improve model accuracy.

Improvements made to phenological states of the entire plant, rather than just the leaf phenology, could enhance representation of water movement through plants under water stress conditions. Different vegetation types have their own root characteristics leading to distinct hydraulic tendencies under variable water regimes and atmospheric conditions, which distinguish whether vegetation is more likely to survive or recover from drought (McDowell et al., 2008; Martínez-Vilalta et al., 2002). Hydraulic strategies may vary by species within a single location (Liu et al., 2020), so the generalization of water-use strategy by PFT in hydrologic models represents the average tendency of vegetation to regulate water. The changing phenological state of root systems likely plays an important role in root water uptake (McCormack et al., 2014). Moreover, models that can account for different vegetation strategies such as the reallocation of carbon storage and below ground respiration during drought may provide a better understanding of mechanisms driving drought resiliency and changes to carbon uptake during drought (Ingrisch et al., 2020; Sanaullah et al., 2012). These types of mechanisms could explain how a warm and wet spring mitigated the effects of the 2012 flash drought on GPP losses (Wolf et al., 2016).

5 Conclusions

To address how water stresses affect carbon and water cycling, we implemented a one-dimensional version of the DCHM-V coupled to a predictive phenology model and analyzed vegetation-atmosphere water and carbon exchanges during flash drought, drought, and non-drought periods. The modeling procedure first required running the DCHM-V with phenology updates from remotely sensed observations of FPAR and LAI. After coupling the predictive phenology model to the DCHM-V, we generated ensembles of model parameters and ran Monte Carlo simulations of the DCHM-PV with concurrent meteorological conditions. We ran three simulations using three distinct assimilation periods for three different sites in Kansas. Uncertainty in model parameters and outputs is reduced when a three year assimilation period, considering average conditions, is used.

The effects of water stress on phenology, infiltration, stomatal conductances, and WUE were similar across all three study sites and helped to distinguish flash drought conditions from non-flash drought conditions. Our findings indicated that both phenology and stomatal conductance play an important role controlling vegetation responses to extreme drought (H2 and H3). Decreased infiltration due to increased days between precipitation during flash drought resulted in less soil water available for plant use (H1 andH2). High vapor pressure deficit led to stomatal closure within the model. With stomata closed, root uptake, transpiration, and carbon assimilation reduced to dormant levels. This led to reductions in WUE during the flash drought that

were more than one standard deviation below other drought periods (H2). FPAR and LAI also reduced during the flash drought but did not exert as strong of a control on reductions in GPP, as observed with changes to stomatal conductance that resulted from increased VPD.

The seasonal timing of the flash drought was particularly detrimental as the rapid dry down occurred during the peak growing
650   season. The amount of water available during the growing season has a major influence on vegetation activity. In this region of the United States, droughts can reduce monthly carbon assimilation by half as compared to non-drought periods while flash droughts are even more detrimental to the overall carbon budget. This has major implications for annual crop yields as well as the carbon uptake capacity for the grasslands and savannas that cover much of the Midwestern US. Future modeling studies should investigate how different vegetation types alter their water-use strategies in response to different water stresses
655   by including (1) adaptive stomatal regulation under elevated VPD, (2) access to deep stores of water in soils and (3) wider ranges of plant functional types and climatological regimes.

Data availability. Results from model simulations are available for download via CUAHSI Hydroshare at https://doi.org/10.4211/hs.331a4e26a36a48928817881a8f3e5db4

Author contributions. LL, TF, and JO originally conceived the idea for this paper. LL designed the methods and supervised implementation
660   by NC. NC carried out all data processing and modeling work. NC and LL analyzed results. NC and LL wrote the manuscript and NC prepared the submissions. All authors contributed to reviewing and editing the manuscript drafts.

Competing interests. The authors declare that no competing interests exist.

Acknowledgements. The authors thank the editor and two anonymous reviewers for their feedback that improved this manuscript. The forcing data used in this study are available from a variety of sources. The NCEP/EMC Stage IV data were acquired from UCAR/NCAR - Earth
665   Observing Laboratory and are avaiable at https://data.eol.ucar.edu/. NLDAS Phase 2, Noah-MP, and SMERGE data used in this study were acquired as part of the mission of NASA's Earth Science Division and archived and distributed by the Goddard Earth Sciences (GES) Data and Information Services Center (DISC). The MODIS MOD15A2H data were retrieved online from Appears and distibuted by NASA Land Processes Distributed Active Archive Center (LP DAAC), http://appeears.earthdatacloud.nasa.gov/. Computations were performed using the Wake Forest University (WFU) High Performance Computing Facility, a centrally managed computational resource available to WFU
670   researchers including faculty, staff, students, and collaborators (Information Systems and Wake Forest University, 2021). Data from this material is stored by CUAHSI via Hydroshare (http://www.hydroshare.org/resource/331a4e26a36a48928817881a8f3e5db4) with support from the National Science Foundation (NSF) Cooperative Agreement No. EAR-1849458. We acknowledge the following AmeriFlux sites for their data records: US-KFS, US-KLS, US-Kon. In addition, funding for AmeriFlux data resources was provided by the US Department

675 of Energy's Office of Science. Maps were generated using data from the US Drought Monitor which is jointly produced by the National Drought Mitigation Center at the University of Nebraska-Lincoln, the United States Department of Agriculture, and the National Oceanic and Atmospheric Administration. This material is based upon work supported by the National Science Foundation under Award Number 2228047.

References

Baldocchi, D., Falge, E., Gu, L., Olson, R., Hollinger, D., Running, S., Anthoni, P., Bernhofer, C., Davis, K., Evans, R., et al.: FLUXNET: A new tool to study the temporal and spatial variability of ecosystem-scale carbon dioxide, water vapor, and energy flux densities, Bulletin of the American Meteorological Society, 82, 2415–2434, 2001.

Baldocchi, D. D.: Assessing the eddy covariance technique for evaluating carbon dioxide exchange rates of ecosystems: past, present and future, Global change biology, 9, 479–492, 2003.

Baldwin, M. and Mitchell, K.: Progress on the NCEP hourly multi-sensor US precipitation analysis for operations and GCIP research, WORLD METEOROLOGICAL ORGANIZATION-PUBLICATIONS-WMO TD, pp. 1–7, 1998.

Barros, A. P.: Adaptive multilevel modeling of land-atmosphere interactions, Journal of climate, 8, 2144–2160, 1995.

Basara, J. B., Christian, J. I., Wakefield, R. A., Otkin, J. A., Hunt, E. H., and Brown, D. P.: The evolution, propagation, and spread of flash drought in the Central United States during 2012, Environmental Research Letters, 14, 084 025, 2019.

Beer, C., Ciais, P., Reichstein, M., Baldocchi, D., Law, B., Papale, D., Soussana, J.-F., Ammann, C., Buchmann, N., Frank, D., et al.: Temporal and among-site variability of inherent water use efficiency at the ecosystem level, Global biogeochemical cycles, 23, 2009.

Brunsell, N.: AmeriFlux BASE US-KFS Kansas Field Station, Ver. 7-5, AmeriFlux AMP, (Dataset), https://doi.org/10.17190/AMF/1246132, 2020a.

Brunsell, N.: AmeriFlux BASE US-Kon Konza Prairie LTER (KNZ), Ver. 5-5, AmeriFlux AMP, (Dataset), https://doi.org/10.17190/AMF/1246068, 2020b.

Brunsell, N.: AmeriFlux BASE US-KLS Kansas Land Institute, Ver. 2-5, AmeriFlux AMP, (Dataset), https://doi.org/10.17190/AMF/1498745, 2021.

Caldararu, S., Purves, D., and Palmer, P.: Phenology as a strategy for carbon optimality: a global model, Biogeosciences, 11, 763–778, 2014.

Chen, J., Jönsson, P., Tamura, M., Gu, Z., Matsushita, B., and Eklundh, L.: A simple method for reconstructing a high-quality NDVI time-series data set based on the Savitzky–Golay filter, Remote sensing of Environment, 91, 332–344, https://doi.org/10.1016/j.rse.2004.03.014, 2004.

Chen, L., Ford, T. W., and Yadav, P.: The Role of Vegetation in Flash Drought Occurrence: A Sensitivity Study Using Community Earth System Model, Version 2, Journal of Hydrometeorology, 22, 845–857, https://doi.org/10.1175/JHM-D-20-0214.1, 2021.

Chen, L. G., Gottschalck, J., Hartman, A., Miskus, D., Tinker, R., and Artusa, A.: Flash drought characteristics based on US drought monitor, Atmosphere, 10, 498, 2019.

Christian, J. I., Basara, J. B., Lowman, L. E., Xiao, X., Mesheske, D., and Zhou, Y.: Flash drought identification from satellite-based land surface water index, Remote Sensing Applications: Society and Environment, 26, 100 770, 2022.

Christian, J. I., Minor, E. R., Basara, J. B., , Furtado, J. C., , Otkin, J. A., Lowman, L. E. L., Hunt, E. D., Mishra, V., and Xiao, X.: Global projections of flash drought show increased risk in a warming climate, Communications Earth and Environment, 4, 165, https://doi.org/10.1038/s43247-023-00826-1, 2023.

Christian, J. I., Hobbins, M., Hoell, A., Otkin, J. A., Ford, T. W., Cravens, A. E., Powlen, K. A., Wang, H., and Mishra, V.: Flash drought: A state of the science review, Wiley Interdisciplinary Reviews: Water, p. e1714, 2024.

Chu, H., Luo, X., Ouyang, Z., Chan, W. S., Dengel, S., Biraud, S. C., Torn, M. S., Metzger, S., Kumar, J., Arain, M. A., et al.: Representativeness of Eddy-Covariance flux footprints for areas surrounding AmeriFlux sites, Agricultural and Forest Meteorology, 301, 108 350, 2021.

715   Cihlar, J., Ly, H., Li, Z., Chen, J., Pokrant, H., and Huang, F.: Multitemporal, multichannel AVHRR data sets for land biosphere studies—artifacts and corrections, Remote sensing of environment, 60, 35–57, https://doi.org/10.1016/S0034-4257(96)00137-X, 1997.

Clausnitzer, V. and Hopmans, J.: Simultaneous modeling of transient three-dimensional root growth and soil water flow, Plant and soil, 164, 299–314, 1994.

Cui, T., Martz, L., and Guo, X.: Grassland phenology response to drought in the Canadian prairies, Remote Sensing, 9, 1258, 2017.

720   Dai, A.: Increasing drought under global warming in observations and models, Nature climate change, 3, 52–58, 2013.

Dai, S., Shulski, M. D., Hubbard, K. G., and Takle, E. S.: A spatiotemporal analysis of Midwest US temperature and precipitation trends during the growing season from 1980 to 2013, International Journal of Climatology, 36, 517–525, 2016.

Devonec, E. and Barros, A. P.: Exploring the transferability of a land-surface hydrology model, Journal of Hydrology, 265, 258–282, 2002.

Dietze, M. C.: Prediction in ecology: A first-principles framework, Ecological Applications, 27, 2048–2060, 2017.

725   Dietze, M. C., Lebauer, D. S., and Kooper, R.: On improving the communication between models and data, Plant, Cell & Environment, 36, 1575–1585, 2013.

Dingman, S. L.: Physical hydrology, Waveland press, 2015.

Du, J.: NCEP/EMC 4KM Gridded Data (GRIB) Stage IV Data. Version 1.0, https://doi.org/10.5065/D6PG1QDD, 2011.

Farquhar, G. D. and Caemmerer, S. v.: Modelling of photosynthetic response to environmental conditions, in: Physiological plant ecology II,
730   pp. 549–587, Springer, 1982.

Farquhar, G. D. and Sharkey, T. D.: Stomatal conductance and photosynthesis, Annual review of plant physiology, 33, 317–345, 1982.

Farquhar, G. D., von Caemmerer, S. v., and Berry, J. A.: A biochemical model of photosynthetic CO2 assimilation in leaves of C3 species, planta, 149, 78–90, 1980.

Flack-Prain, S., Meir, P., Malhi, Y., Smallman, T. L., and Williams, M.: The importance of physiological, structural and trait responses to
735   drought stress in driving spatial and temporal variation in GPP across Amazon forests, Biogeosciences, 16, 4463–4484, 2019.

Ford, T. W. and Labosier, C. F.: Meteorological conditions associated with the onset of flash drought in the eastern United States, Agricultural and forest meteorology, 247, 414–423, https://doi.org/10.1016/j.agrformet.2017.08.031, 2017.

Friedl, M. and Sulla-Menashe, D.: MCD12Q1 MODIS, Terra+ Aqua Land cover type yearly L3 global 500m SIN grid, 6, 2015.

Garcia-Forner, N., Biel, C., Savé, R., and Martínez-Vilalta, J.: Isohydric species are not necessarily more carbon limited than anisohydric
740   species during drought, Tree physiology, 37, 441–455, 2017.

Garcia-Quijano, J. F. and Barros, A. P.: Incorporating canopy physiology into a hydrological model: photosynthesis, dynamic respiration, and stomatal sensitivity, Ecological Modelling, 185, 29–49, 2005.

Gebremichael, M. and Barros, A. P.: Evaluation of MODIS gross primary productivity (GPP) in tropical monsoon regions, Remote Sensing of Environment, 100, 150–166, 2006.

745   Gerken, T., Bromley, G. T., Ruddell, B. L., Williams, S., and Stoy, P. C.: Convective suppression before and during the United States Northern Great Plains flash drought of 2017, Hydrology and Earth System Sciences, 22, 4155–4163, 2018.

Giardina, F., Gentine, P., Konings, A. G., Seneviratne, S. I., and Stocker, B. D.: Diagnosing evapotranspiration responses to water deficit across biomes using deep learning, New Phytologist, 2023.

Grossiord, C., Buckley, T. N., Cernusak, L. A., Novick, K. A., Poulter, B., Siegwolf, R. T., Sperry, J. S., and McDowell, N. G.: Plant responses
750   to rising vapor pressure deficit, New Phytologist, 226, 1550–1566, 2020.

Guo, J. S., Hultine, K. R., Koch, G. W., Kropp, H., and Ogle, K.: Temporal shifts in iso/anisohydry revealed from daily observations of plant water potential in a dominant desert shrub, New Phytologist, 225, 713–726, 2020.

Guo, J. S., Bush, S. E., and Hultine, K. R.: Temporal variation in stomatal sensitivity to vapour pressure deficit in western riparian forests, Functional Ecology, 36, 1599–1611, 2022.

755 He, M., Kimball, J. S., Yi, Y., Running, S., Guan, K., Jensco, K., Maxwell, B., and Maneta, M.: Impacts of the 2017 flash drought in the US Northern plains informed by satellite-based evapotranspiration and solar-induced fluorescence, Environmental Research Letters, 14, 074 019, https://doi.org/10.1088/1748-9326/ab22c3, 2019.

He, W., Ju, W., Schwalm, C. R., Sippel, S., Wu, X., He, Q., Song, L., Zhang, C., Li, J., Sitch, S., et al.: Large-scale droughts responsible for dramatic reductions of terrestrial net carbon uptake over North America in 2011 and 2012, Journal of Geophysical Research:
760   Biogeosciences, 123, 2053–2071, https://doi.org/10.1029/2018JG004520, 2018.

Heinsch, F. A., Zhao, M., Running, S. W., Kimball, J. S., Nemani, R. R., Davis, K. J., Bolstad, P. V., Cook, B. D., Desai, A. R., Ricciuto, D. M., et al.: Evaluation of remote sensing based terrestrial productivity from MODIS using regional tower eddy flux network observations, IEEE transactions on geoscience and remote sensing, 44, 1908–1925, 2006.

Hochberg, U., Rockwell, F. E., Holbrook, N. M., and Cochard, H.: Iso/anisohydry: a plant–environment interaction rather than a simple
765   hydraulic trait, Trends in plant science, 23, 112–120, 2018.

Hosseini, A., Mocko, D. M., Brunsell, N., Kumar, S. V., Mahanama, S. P., Arsenault, K., and Roundy, J.: Understanding the Impact of Vegetation Dynamics on the Water Cycle in the Noah-MP Model, Frontiers in Water, p. 136, 2022.

Hu, Z., Yu, G., Fu, Y., Sun, X., Li, Y., Shi, P., Wang, Y., and Zheng, Z.: Effects of vegetation control on ecosystem water use efficiency within and among four grassland ecosystems in China, Global Change Biology, 14, 1609–1619, 2008.

770 Hunt, E. D., Svoboda, M., Wardlow, B., Hubbard, K., Hayes, M., and Arkebauer, T.: Monitoring the effects of rapid onset of drought on non-irrigated maize with agronomic data and climate-based drought indices, Agricultural and Forest Meteorology, 191, 1–11, 2014.

Information Systems and Wake Forest University: WFU High Performance Computing Facility, https://doi.org/10.57682/G13Z-2362, 2021.

Ingrisch, J., Karlowsky, S., Hasibeder, R., Gleixner, G., and Bahn, M.: Drought and recovery effects on belowground respiration dynamics and the partitioning of recent carbon in managed and abandoned grassland, Global Change Biology, 26, 4366–4378, 2020.

775 Jackson, R. B., Canadell, J., Ehleringer, J. R., Mooney, H., Sala, O., and Schulze, E.-D.: A global analysis of root distributions for terrestrial biomes, Oecologia, 108, 389–411, 1996.

Jin, C., Luo, X., Xiao, X., Dong, J., Li, X., Yang, J., and Zhao, D.: The 2012 flash drought threatened US Midwest agroecosystems, Chinese Geographical Science, 29, 768–783, https://doi.org/10.1007/s11769-019-1066-7, 2019.

Jolly, W. M., Nemani, R., and Running, S. W.: A generalized, bioclimatic index to predict foliar phenology in response to climate, Global
780   Change Biology, 11, 619–632, 2005.

Kannenberg, S. A., Guo, J. S., Novick, K. A., Anderegg, W. R., Feng, X., Kennedy, D., Konings, A. G., Martínez-Vilalta, J., and Matheny, A. M.: Opportunities, challenges and pitfalls in characterizing plant water-use strategies, Functional Ecology, 36, 24–37, 2022.

Katul, G., Lai, C.-T., Schäfer, K., Vidakovic, B., Albertson, J., Ellsworth, D., and Oren, R.: Multiscale analysis of vegetation surface fluxes: from seconds to years, Advances in Water Resources, 24, 1119–1132, 2001.

785 Kim, Y., Moorcroft, P., Aleinov, I., Puma, M., and Kiang, N.: Variability of phenology and fluxes of water and carbon with observed and simulated soil moisture in the Ent Terrestrial Biosphere Model (Ent TBM version 1.0. 1.0. 0), Geoscientific Model Development, 8, 3837–3865, 2015.

Kimball, J. S., Jones, L., Jensco, K., He, M., Maneta, M., and Reichle, R.: SMAP L4 assessment of the US northern plains 2017 flash drought, in: IGARSS 2019-2019 IEEE International Geoscience and Remote Sensing Symposium, pp. 5366–5369, IEEE, 2019.

790 Kirono, D. G., Round, V., Heady, C., Chiew, F. H., and Osbrough, S.: Drought projections for Australia: Updated results and analysis of model simulations, Weather and Climate Extremes, 30, 100 280, 2020.

Konings, A. G. and Gentine, P.: Global variations in ecosystem-scale isohydricity, Global change biology, 23, 891–905, 2017.

Kumar, S. V., Mocko, D. M., Wang, S., Peters-Lidard, C. D., and Borak, J.: Assimilation of remotely sensed leaf area index into the Noah-MP land surface model: Impacts on water and carbon fluxes and states over the continental United States, Journal of Hydrometeorology, 20,

795 1359–1377, 2019.

Lai, C.-T. and Katul, G.: The dynamic role of root-water uptake in coupling potential to actual transpiration, Advances in Water Resources, 23, 427–439, 2000.

Lawson, T. and Vialet-Chabrand, S.: Speedy stomata, photosynthesis and plant water use efficiency, New Phytologist, 221, 93–98, 2019.

Li, L., Yang, Z.-L., Matheny, A. M., Zheng, H., Swenson, S. C., Lawrence, D. M., Barlage, M., Yan, B., McDowell, N. G., and Leung,

800 L. R.: Representation of plant hydraulics in the Noah-MP land surface model: Model development and multiscale evaluation, Journal of Advances in Modeling Earth Systems, 13, e2020MS002 214, 2021.

Lisonbee, J., Woloszyn, M., and Skumanich, M.: Making sense of flash drought: Definitions, indicators, and where we go from here, J. Appl. Serv. Climatol, 2021, 1–19, https://doi.org/10.46275/JOASC.2021.02.001, 2021.

Liu, Y., Kumar, M., Katul, G. G., Feng, X., and Konings, A. G.: Plant hydraulics accentuates the effect of atmospheric moisture stress on

805 transpiration, Nature Climate Change, 10, 691–695, 2020.

Lowman, L. E. and Barros, A. P.: Interplay of drought and tropical cyclone activity in SE US gross primary productivity, Journal of Geophysical Research: Biogeosciences, 121, 1540–1567, https://doi.org/10.1002/2015JG003279, 2016.

Lowman, L. E. and Barros, A. P.: Predicting canopy biophysical properties and sensitivity of plant carbon uptake to water limitations with a coupled eco-hydrological framework, Ecological Modelling, 372, 33–52, 2018.

810 Lowman, L. E., Christian, J. I., and Hunt, E. D.: How land surface characteristics influence the development of flash drought through the drivers of soil moisture and vapor pressure deficit, Journal of Hydrometeorology, 2023.

Martínez-Vilalta, J., Piñol, J., and Beven, K.: A hydraulic model to predict drought-induced mortality in woody plants: an application to climate change in the Mediterranean, Ecological Modelling, 155, 127–147, 2002.

McCormack, M. L., Adams, T. S., Smithwick, E. A., and Eissenstat, D. M.: Variability in root production, phenology, and turnover rate

815 among 12 temperate tree species, Ecology, 95, 2224–2235, 2014.

McDowell, N., Pockman, W. T., Allen, C. D., Breshears, D. D., Cobb, N., Kolb, T., Plaut, J., Sperry, J., West, A., Williams, D. G., et al.: Mechanisms of plant survival and mortality during drought: why do some plants survive while others succumb to drought?, New phytologist, 178, 719–739, 2008.

Meinzer, F. C.: Co-ordination of vapour and liquid phase water transport properties in plants, Plant, Cell & Environment, 25, 265–274, 2002.

820 Miller, D. A. and White, R. A.: A conterminous United States multilayer soil characteristics dataset for regional climate and hydrology modeling, Earth interactions, 2, 1–26, 1998.

Mitchell, K. E., Lohmann, D., Houser, P. R., Wood, E. F., Schaake, J. C., Robock, A., Cosgrove, B. A., Sheffield, J., Duan, Q., Luo, L., et al.: The multi-institution North American Land Data Assimilation System (NLDAS): Utilizing multiple GCIP products and partners in a continental distributed hydrological modeling system, Journal of Geophysical Research: Atmospheres, 109, 2004.

825 Mocko, D. M., Kumar, S. V., Peters-Lidard, C. D., and Wang, S.: Assimilation of vegetation conditions improves the representation of drought over agricultural areas, Journal of Hydrometeorology, 22, 1085–1098, 2021.

Moradkhani, H., Sorooshian, S., Gupta, H. V., and Houser, P. R.: Dual state–parameter estimation of hydrological models using ensemble Kalman filter, Advances in water resources, 28, 135–147, https://doi.org/10.1016/j.advwatres.2004.09.002, 2005.

Myneni, R., Knyazikhin, Y., and Park, T.: MOD15A2H MODIS/Terra leaf area Index/FPAR 8-Day L4 global 500m SIN grid V006, NASA EOSDIS Land Processes DAAC, 2015.

Novick, K. A., Ficklin, D. L., Stoy, P. C., Williams, C. A., Bohrer, G., Oishi, A. C., Papuga, S. A., Blanken, P. D., Noormets, A., Sulman, B. N., et al.: The increasing importance of atmospheric demand for ecosystem water and carbon fluxes, Nature climate change, 6, 1023–1027, 2016.

Otkin, J. A., Anderson, M. C., Hain, C., Svoboda, M., Johnson, D., Mueller, R., Tadesse, T., Wardlow, B., and Brown, J.: Assessing the evolution of soil moisture and vegetation conditions during the 2012 United States flash drought, Agricultural and forest meteorology, 218, 230–242, https://doi.org/10.1016/j.agrformet.2015.12.065, 2016.

Otkin, J. A., Svoboda, M., Hunt, E. D., Ford, T. W., Anderson, M. C., Hain, C., and Basara, J. B.: Flash droughts: A review and assessment of the challenges imposed by rapid-onset droughts in the United States, Bulletin of the American Meteorological Society, 99, 911–919, https://doi.org/10.1175/BAMS-D-17-0149.1, 2018.

Otkin, J. A., Woloszyn, M., Wang, H., Svoboda, M., Skumanich, M., Pulwarty, R., Lisonbee, J., Hoell, A., Hobbins, M., Haigh, T., et al.: Getting ahead of Flash Drought: From Early Warning to Early Action, Bulletin of the American Meteorological Society, 103, E2188–E2202, 2022.

Pastorello, G., Trotta, C., Canfora, E., Chu, H., Christianson, D., Cheah, Y.-W., Poindexter, C., Chen, J., Elbashandy, A., Humphrey, M., et al.: The FLUXNET2015 dataset and the ONEFlux processing pipeline for eddy covariance data, Scientific data, 7, 1–27, 2020.

Pearson, R. G., Phillips, S. J., Loranty, M. M., Beck, P. S., Damoulas, T., Knight, S. J., and Goetz, S. J.: Shifts in Arctic vegetation and associated feedbacks under climate change, Nature climate change, 3, 673–677, 2013.

Poonia, V., Goyal, M. K., Jha, S., and Dubey, S.: Terrestrial ecosystem response to flash droughts over India, Journal of Hydrology, 605, 127 402, 2022.

Qing, Y., Wang, S., Ancell, B. C., and Yang, Z.-L.: Accelerating flash droughts induced by the joint influence of soil moisture depletion and atmospheric aridity, Nature communications, 13, 1–10, 2022.

Roman, D., Novick, K., Brzostek, E., Dragoni, D., Rahman, F., and Phillips, R.: The role of isohydric and anisohydric species in determining ecosystem-scale response to severe drought, Oecologia, 179, 641–654, 2015.

Running, S., Mu, Q., and Zhao, M.: MOD17A2H MODIS/terra gross primary productivity 8-day L4 global 500m SIN grid V006, NASA EOSDIS Land Processes DAAC, 2015.

Running, S. W., Nemani, R. R., Heinsch, F. A., Zhao, M., Reeves, M., and Hashimoto, H.: A continuous satellite-derived measure of global terrestrial primary production, Bioscience, 54, 547–560, 2004.

Sade, N., Gebremedhin, A., and Moshelion, M.: Risk-taking plants: anisohydric behavior as a stress-resistance trait, Plant signaling & behavior, 7, 767–770, 2012.

Sanaullah, M., Chabbi, A., Rumpel, C., and Kuzyakov, Y.: Carbon allocation in grassland communities under drought stress followed by 14C pulse labeling, Soil Biology and Biochemistry, 55, 132–139, 2012.

Savitzky, A. and Golay, M. J.: Smoothing and differentiation of data by simplified least squares procedures., Analytical chemistry, 36, 1627–1639, 1964.

Schmid, H.: Source areas for scalars and scalar fluxes, Boundary-Layer Meteorology, 67, 293–318, 1994.

Sellers, P. J., Dickinson, R., Randall, D., Betts, A. K., Hall, F. G., Berry, J. A., Collatz, G., Denning, A., Mooney, H. A., Nobre, C. A., et al.:
865 Modeling the exchanges of energy, water, and carbon between continents and the atmosphere, Science, 275, 502–509, 1997.

Soil Survey Staff, Natural Resources Conservation Service, U. S. D. o. A.: Web Soil Survey. Available online. Accessed 07 December 2022,
https://www.nrcs.usda.gov/resources/data-and-reports/web-soil-survey.

Stöckli, R., Rutishauser, T., Dragoni, D., O'keefe, J., Thornton, P., Jolly, M., Lu, L., and Denning, A.: Remote sensing data assimilation for
a prognostic phenology model, Journal of Geophysical Research: Biogeosciences, 113, https://doi.org/10.1029/2008JG000781, 2008.

870 Sulla-Menashe, D. and Friedl, M. A.: User guide to collection 6 MODIS land cover (MCD12Q1 and MCD12C1) product, USGS: Reston,
VA, USA, 1, 18, 2018.

Svoboda, M., LeComte, D., Hayes, M., Heim, R., Gleason, K., Angel, J., Rippey, B., Tinker, R., Palecki, M., Stooksbury, D., et al.: The
drought monitor, Bulletin of the American Meteorological Society, 83, 1181–1190, 2002.

Tanré, D., Kaufman, Y., Herman, M., and Mattoo, S.: Remote sensing of aerosol properties over oceans using the MODIS/EOS spectral
875 radiances, Journal of Geophysical Research: Atmospheres, 102, 16 971–16 988, https://doi.org/10.1029/96JD03437, 1997.

Tao, J. and Barros, A.: Coupled prediction of flood response and debris flow initiation during warm-and cold-season events in the Southern
Appalachians, USA, Hydrology and Earth System Sciences, 18, 367–388, 2014.

Tao, J. and Barros, A. P.: Prospects for flash flood forecasting in mountainous regions–An investigation of Tropical Storm Fay in the Southern
Appalachians, Journal of Hydrology, 506, 69–89, 2013.

880 Thornthwaite, C. W. and Mather, J. R.: Instructions and tables for computing potential evapotranspiration and the water balance., Publications
on Climatology, 10, 185–310, 1957.

Tobin, K. J., Bennett, M. E., and Torres, R.: Long-term root zone moisture trends across CONUS from a new root-zone soil moisture product
called SMERGE, in: AGU Fall Meeting Abstracts, vol. 2019, pp. H51S–1750, 2019.

Towne, G. and Owensby, C.: Long-term effects of annual burning at different dates in ungrazed Kansas tallgrass prairie., Rangeland Ecology
885 & Management/Journal of Range Management Archives, 37, 392–397, 1984.

Trenberth, K. E., Dai, A., Van Der Schrier, G., Jones, P. D., Barichivich, J., Briffa, K. R., and Sheffield, J.: Global warming and changes in
drought, Nature Climate Change, 4, 17–22, 2014.

Urban, J., Ingwers, M., McGuire, M. A., and Teskey, R. O.: Stomatal conductance increases with rising temperature, Plant signaling &
behavior, 12, e1356 534, 2017.

890 Vargas Zeppetello, L. R., McColl, K. A., Bernau, J. A., Bowen, B. B., Tang, L. I., Holbrook, N. M., Gentine, P., and Huybers, P.: Apparent
surface conductance sensitivity to vapour pressure deficit in the absence of plants, Nature Water, pp. 1–11, 2023.

Wang, J., Rich, P. M., and Price, K. P.: Temporal responses of NDVI to precipitation and temperature in the central Great Plains, USA,
International journal of remote sensing, 24, 2345–2364, 2003.

Wolf, S., Keenan, T. F., Fisher, J. B., Baldocchi, D. D., Desai, A. R., Richardson, A. D., Scott, R. L., Law, B. E., Litvak, M. E., Brunsell, N. A.,
895 et al.: Warm spring reduced carbon cycle impact of the 2012 US summer drought, Proceedings of the National Academy of Sciences, 113,
5880–5885, 2016.

Wu, G., Guan, K., Li, Y., Novick, K. A., Feng, X., McDowell, N. G., Konings, A. G., Thompson, S. E., Kimball, J. S., De Kauwe, M. G.,
et al.: Interannual variability of ecosystem iso/anisohydry is regulated by environmental dryness, New Phytologist, 229, 2562–2575, 2021.

Xia, Y., Mitchell, K., Ek, M., Sheffield, J., Cosgrove, B., Wood, E., Luo, L., Alonge, C., Wei, H., Meng, J., et al.: Continental-scale water
900 and energy flux analysis and validation for the North American Land Data Assimilation System project phase 2 (NLDAS-2): 1. Intercomparison and application of model products, Journal of Geophysical Research: Atmospheres, 117, 2012.

Xu, T., Chen, F., He, X., Barlage, M., Zhang, Z., Liu, S., and He, X.: Improve the performance of the noah-MP-crop model by jointly assimilating soil moisture and vegetation phenology data, Journal of Advances in Modeling Earth Systems, 13, e2020MS002 394, 2021.

Yan, K., Park, T., Yan, G., Chen, C., Yang, B., Liu, Z., Nemani, R. R., Knyazikhin, Y., and Myneni, R. B.: Evaluation of MODIS LAI/FPAR product collection 6. Part 1: Consistency and improvements, Remote Sensing, 8, 359, 2016.

Yao, T., Liu, S., Hu, S., and Mo, X.: Response of vegetation ecosystems to flash drought with solar-induced chlorophyll fluorescence over the Hai River Basin, China during 2001–2019, Journal of Environmental Management, 313, 114 947, 2022.

Yildiz, O. and Barros, A. P.: Climate variability, water resources, and hydrologic extremes—Modeling the water and energy budgets, Climate and Hydrology, in Mountain Areas, pp. 291–306, 2005.

Yildiz, O. and Barros, A. P.: Elucidating vegetation controls on the hydroclimatology of a mid-latitude basin, Journal of Hydrology, 333, 431–448, 2007.

Yildiz, O., Barros, A. P., et al.: Evaluating spatial variability and scale effects on hydrologic processes in a midsize river basin, Sci. Res. Essays, 4, 217–225, 2009.

Zeng, X.: Global vegetation root distribution for land modeling, Journal of Hydrometeorology, 2, 525–530, 2001.

Zeng, Z., Wu, W., Li, Y., Huang, C., Zhang, X., Peñuelas, J., Zhang, Y., Gentine, P., Li, Z., Wang, X., et al.: Increasing meteorological drought under climate change reduces terrestrial ecosystem productivity and carbon storage, One Earth, 6, 1326–1339, 2023.

Zhang, M. and Yuan, X.: Rapid reduction in ecosystem productivity caused by flash droughts based on decade-long FLUXNET observations, Hydrology and Earth System Sciences, 24, 5579–5593, 2020.

Zhang, M., Yuan, X., and Otkin, J. A.: Remote sensing of the impact of flash drought events on terrestrial carbon dynamics over China, Carbon Balance and Management, 15, 1–11, https://doi.org/10.1186/s13021-020-00156-1, 2020.

Zhou, S., Duursma, R. A., Medlyn, B. E., Kelly, J. W., and Prentice, I. C.: How should we model plant responses to drought? An analysis of stomatal and non-stomatal responses to water stress, Agricultural and Forest Meteorology, 182, 204–214, 2013.